Chemical Physics Reviews ARTICLE scitation.org/journal/cpr

Quantization effects in semiconductor nanostructures and singlet fission in molecular chromophores for photovoltaics and solar fuels

Cite as: Chem. Phys. Rev. **2**, 021305 (2021); doi: 10.1063/5.0028982
Submitted: 8 September 2020 · Accepted: 11 May 2021 ·
Published Online: 15 June 2021

View Online Export Citation CrossMark

Arthur J. Nozik[a)]

AFFILIATIONS

Boulder Department of Chemistry and RASEI, University of Colorado, Boulder, Colorado 80309, USA and National Renewable Energy Laboratory, Golden, Colorado 80401, USA

[a)]Author to whom correspondence should be addressed: arthur.nozik@colorado.edu

ABSTRACT

Hot carriers in semiconductors are electrons and/or holes that have energies greater than carriers that reside at the top and bottom of the conduction and valence bands, respectively; the latter carriers are in equilibrium with the lattice and have a temperature equal to the lattice (ambient) temperature. Hot carriers are created in semiconductors upon the absorption of photons with energies greater than the bandgap. The excess energy above the bandgap energy is in the form of kinetic energy. The hot carriers can cool to the lattice temperature via electron–phonon scattering and establish separate Boltzmann distributions for electrons and holes at the band edges. Thus, upon cooling, the excess kinetic energy of the hot carriers is transformed into heat and is unavailable to be converted into electrical or chemical free energy in a solar photon-converting cell. This hot-carrier cooling process significantly limits the maximum possible power conversion efficiency (PCE) of the free energy of solar photons into electrical free energy or chemical free energy in chemical bonds of fuels. However, if hot-carrier cooling can be slowed such that the hot carriers can be extracted before cooling to create higher photovoltages, or utilized to create additional electron-hole pairs through carrier multiplication, then beneficial use can be made of the excess energy of hot carriers and the maximum thermodynamic PCE can be dramatically increased. Quantization effects in semiconductor nanostructures, unique properties of some bulk semiconductors, and exciton multiplication in both semiconductors and molecular chromophores that undergo singlet fission have shown a path forward for potential dramatic increases in the PCEs of solar photons into electricity and solar fuels. The status, history, and future promise of the science and technology of these future approaches for different types of photovoltaic cells and cells for solar fuels will be discussed.

TABLE OF CONTENTS

I. INTRODUCTION AND FUNDAMENTALS

A. Formation and cooling of hot carriers in semiconductors and singlet fission in molecules

When a photon is absorbed in a crystalline bulk semiconductor with an energy greater than the bandgap, an electron-hole pair is formed.[1–4] The distribution of the excess photon energy between photogenerated electrons in the conduction band and photogenerated holes in the valence band depends upon the effective masses of these charge carriers; the carriers having the smallest effective mass retain the greatest fraction of the excess photon energy. For moderate photon energies in excess of the bandgap (less than ∼100 meV) and for parabolic bands, the distribution of the excess energy above the bandgap energy between the photogenerated electron and hole is given by

$$\Delta E_e = \left(h\nu - E_g\right)\left[1 + m_e^*/m_h^*\right]^{-1} \quad (1)$$

and

$$\Delta E_h = \left(h\nu - E_g\right) - \Delta E_e, \quad (2)$$

where m_e^* and m_h^* are the effective masses of electrons and holes, respectively, ΔE_e is the energy difference between the initial energy of the photogenerated electron and the energy of the conduction band edge, and ΔE_h is the energy difference between the initial photogenerated hole energy and the valence band edge (Fig. 1).[1–3] The excess energies of the photogenerated electrons and holes are in the form of kinetic energy and both these charge carriers are far from equilibrium; they are termed hot carriers because their energies are higher than the energies of thermally equilibrated electrons and holes that exist within kT of their respective band edges.[1,4–12] Generally, the non-equilibrium condition passes through 4 successive stages to reach equilibrium: (1) initially at t = 0, the photogenerated hot electrons and holes exist as

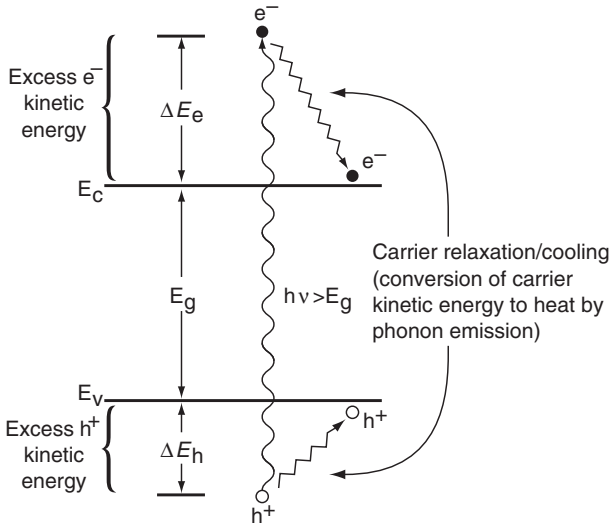

FIG 1. Hot-carrier relaxation/cooling in semiconductors. Reprinted with permission from A. J. Nozik, Annu. Rev. Phys. Chem. **52**, 193–231 (2001). Copyright 2001 Annual Reviews, Inc.[1]

two separate populations, both non-equilibrated (meaning they both cannot be assigned carrier temperatures); (2) after less than ∼100 fs the initial population of high energy carriers and native cold carriers equilibrate among themselves via separate electron–electron and hole–hole scattering; if the inter-carrier scattering is stronger than external forces that could continue to drive non-equilibrium, the two-carrier populations can form two separate Boltzmann distributions with two hot-carrier temperatures defined for both photogenerated electrons and holes (no energy has been lost at this point); (3) at later times of the order of ps or less, the hot electrons and/or holes interact with phonons (lattice vibrations of the semiconductor atoms) to dissipate the excess kinetic energy as heat via phonon emission and reach the lattice temperature (i.e., the ambient temperature which is lower than the initial hot-electron and hot-hole temperatures); and finally, (4) after time scales ranging from nanoseconds to microseconds, the excess photogenerated electrons and holes recombine through radiative and non-radiative channels to bring the carrier density back to its original condition in the dark before photoexcitation.[1]

Hot carriers can be photogenerated by the absorption of either supra-bandgap light pulses or via steady-state illumination. For continuous optical excitation, a steady-state population of excited, non-equilibrated carriers is produced; the characteristics of this steady-state population depends upon the balance between the rate and energetics of carrier photogeneration and the kinetics of the various equilibration pathways.

The dynamics of hot-carrier formation and relaxation to equilibrium is more easily discussed within the context of pulsed excitation of monochromatic light. If photon absorption produces electrons and holes, each with initial excess kinetic energies at least kT above the conduction and valence bands, then both initial carrier temperatures are always above the lattice temperature—hence, the term hot carriers (hot electrons and hot holes).[1]

Equilibration of the hot carriers with the lattice (i.e., carrier cooling) is achieved through carrier-phonon scattering (phonon emission

through interactions with electrons and/or holes); at high hot-carrier energies, the cooling involves longitudinal optical (LO) phonons and at lower carrier temperatures, acoustic phonons are involved. The cooling may occur by each carrier undergoing a stepwise cascade of interactions with phonons or in an Auger process in which the excess energy of one carrier type is transferred to the other type, which then undergoes faster phonon scattering. These processes produce carrier cooling; some researchers refer to cooling as carrier thermalization, but this latter terminology can cause confusion with the first stage of equilibration described above that establishes a Boltzmann distribution among the carriers.[1] Hence, we restrict the term thermalization to the first stage of carrier relaxation and refer to the second stage that involves carrier-phonon interactions as carrier cooling.[1] Another possible important process that could follow the photoexcitation of semiconductors is spatial separation and transport of the photogenerated electrons and holes. The separated photogenerated carriers can subsequently be collected in a photoconversion device to generate a photovoltage and a photocurrent (photovoltaic effect);[1,4–10] or alternatively, the separated carriers can drive coupled electrochemical oxidation and reduction reactions (generally called redox reactions) at a semiconductor-electrolyte interface; this latter process is termed photoelectrochemical energy conversion (PEC).[8] Photoelectrochemistry can drive endoergic electrochemical reactions uphill in energy thereby forming chemical fuels (a positive free energy change) or they can drive exoergic reactions downhill (a negative free energy change) that is frequently termed photocatalysis (there is some ambiguity in the latter nomenclature since driving an endoergic reaction uphill faster could also be considered photocatalysis).[1,8]

Applications that involve conversion of radiant energy to electrical or positive chemical free energy changes have an ultimate thermodynamic limit on the conversion efficiency (first derived by Shockley and Queisser[4]) of about 33% for carriers fully equilibrated with the lattice in a single threshold (single bandgap) semiconductor photoconverter.[4] However, this conversion efficiency can be increased theoretically to about 66% for photoconversion utilizing hot carriers that have not undergone any degree of cooling via interaction with phonons and are therefore converted at their initial hot-carrier temperatures.[1,8–10]

Two fundamental ways exist to utilize hot carriers for enhancing the efficiency of photon conversion in semiconductors. One way produces a higher photopotential (photovoltage) for useful work and the second way produces a higher photocurrent. The former requires that the hot carriers be extracted from the photoconverter to do useful work before they cool,[1,8–12] whereas the latter requires the hot carriers to produce a second (or more) electron-hole pair through carrier multiplication[12–31] (a process labeled impact ionization in bulk semiconductors[1,2]). This latter process is the inverse of an Auger process whereby one of two electron-hole pairs recombine and pass the recombination energy to the remaining electron-hole pair to produce a single highly energetic electron-hole pair. To achieve the hot-carrier extraction process, the rates of photogenerated carrier separation, transport, and interfacial charge transfer across the semiconductor-molecule interface must all be fast compared to the rate of hot-carrier cooling. The hot-carrier process of carrier multiplication requires that the rate of multiplication be greater than the rate of carrier cooling and other possible competing carrier relaxation, transport, and trapping processes.[1]

Because hot electrons and hot holes in conventional semiconductors used for photovoltaic (PV) solar cells usually have different effective masses, they generally cool at different rates; for most inorganic semiconductors, the effective masses of electrons are significantly lighter than holes and therefore, electrons cool more slowly. Another important factor for hot-carrier cooling dynamics is that the cooling rates are dependent upon the photogenerated density of hot carriers (i.e., the absorbed light intensity).[1,32–34] Since most of the dynamical effects we discuss here are dominated by electrons rather than holes, we limit our subsequent discussion of hot-carrier dynamics primarily to the relaxation dynamics of photogenerated hot electrons.

A very important scientific development regarding the relaxation dynamics of hot carriers in semiconductors has been the proposal and experimental verification[1,9,11–34] that the relaxation dynamics may be dramatically altered by quantization effects in semiconductors (i.e., in semiconductor quantum wells, quantum wires, quantum dots, superlattices, and nanostructures/nanocrystals). Namely, when hot carriers in the semiconductor are confined by potential barriers to regions of space that are smaller than or comparable to their de Broglie wavelength or to the Bohr radius of excitons in the semiconductor bulk, their relaxation dynamics and pathways can be dramatically affected; specifically, the hot-carrier cooling rates may be greatly reduced and the rate of carrier multiplication could be enhanced and exceed the rate of hot-carrier cooling.[1,11–34] In these quantum-confined semiconductor nanostructures, the electrons and holes are squeezed together so closely that they become correlated and form excitons, even at room temperature, and the process of carrier multiplication is then called multiple exciton generation (MEG).[14]

Finally, also in recent years, an analogous effect to MEG has been recognized in molecular chromophores; this photochemical process in molecular chromophores is termed singlet fission (SF).[35–40] Singlet fission can occur in dimolecular chromophores that have a triple-state energy (T_1) that is close to $\frac{1}{2}$ the energy of the first allowed optical transition ($S_0 - S_1$); upon photoexcitation to S_1 exciton, multiplication can occur producing two triplet states from the singlet state.[35–40] The two triplet states can then undergo charge separation resulting in two electrons and two positive holes that move in opposite directions and are separately collected in photoconversion devices that will enhance the photocurrent by creating two charge carriers per absorbed single photon. Furthermore, the SF process has been shown to have a total quantum yield of 200% at the photon energy where it is approximately twice the HOMO–LUMO transition energy, thus maximizing the power conversion efficiency of these absorbed photons. The SF exciton multiplication process requires that the molecular entity consists of two monomers that are appropriately electronically coupled in either a dimer or oligomer configuration, or as two monomers closely coupled as neighbors in a molecular crystal. SF is thus a spin-allowed process since the coupled electronic configuration of the two triplets is a singlet. Figs. 2(a) and 2(b) show the energetics and overall process of SF.[35–40]

B. Quantization effects in semiconductors

Quantization effects begin to occur in typical semiconductors (Groups IV, III-V, II-VI, and IV-VI) when their physical dimensions range from about 2 to 20 nm. In general, charge carriers in semiconductors can be confined by potential barriers in one, two, or three spatial dimensions (Fig. 3); specifically, at least one of the three

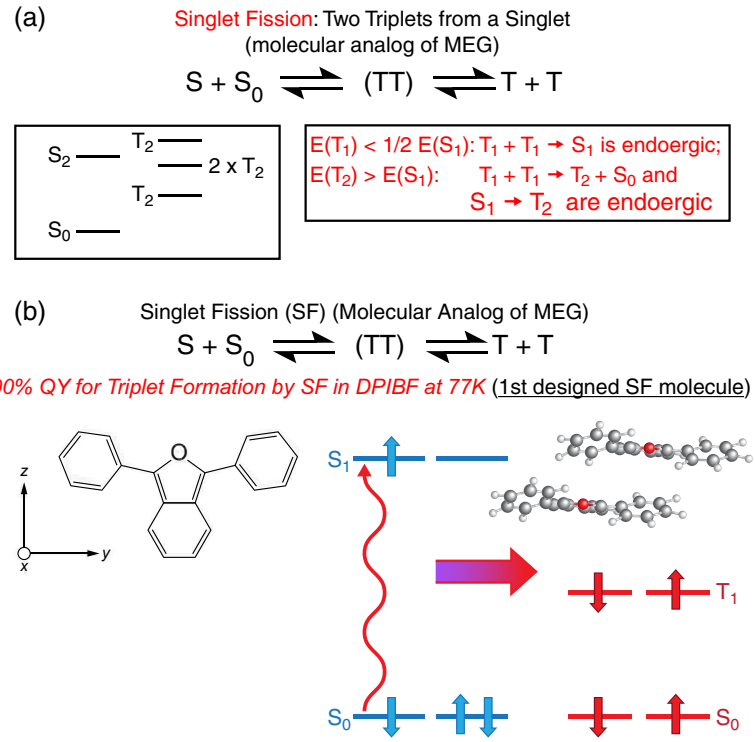

FIG. 2. (a) Energetics of singlet fission. For SF to occur in molecules, its triplet state T_1 needs to be about $^1/_2$ the energy of $S_1 - S_0$. Reprinted with permission from Smith and Michl, Chem. Rev. **110**, 6891–6936 (2010). Copyright 2010 American Chemical Society.[36] (b) Net result of singlet fission for diphenylisobenzofuran (DPIBF). Two identical molecular entities need to interact so that the photogenerated double-triplet state is spin-allowed. Reprinted with permission from Johnson *et al.*, Accts. Chem. Res. **46**(6), 1290–1299 (2013). Copyright 2013 American Chemical Society.[150]

dimensions needs to have its size comparable to or less than the Bohr radius of excitons in that material; alternatively, the size must be smaller than the de Broglie wavelength of electrons in that material. The number of the three spatial dimensions satisfying the size criteria indicated above define the three regimes of quantum confinement. These three regimes are termed quantum films, quantum wires (Qwires), and quantum dots (QDs), respectively.[1]

When quantization effects in semiconductors were first studied beginning in the 1970s, they were formed as 1-dimensionally confined quantum films and were referred to as quantum wells (QWs), multiple quantum wells (MQWs), single quantum wells (SQWs), or superlattices (SLs), depending upon the number of well layers and the barrier thicknesses.[41–43] They were produced by molecular beam epitaxy (MBE) and metallo-organic chemical vapor deposition (MOCVD);[1] the generated quantum films represented textbook examples of one-dimensional quantum wells.[41–43] Figure 4 shows the resultant density of states (DOS) for the different degrees of quantum confinement.[1]

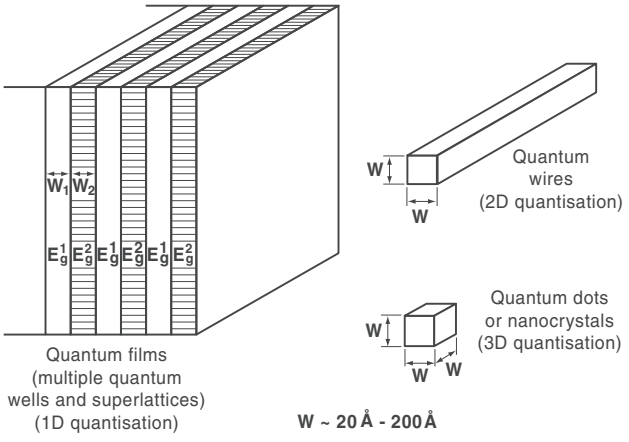

FIG. 3. Three quantization configurations depending on whether the confinement is in 1, 2, or 3 dimensions. Reprinted with permission from A. J. Nozik, Annu. Rev. Phys. Chem. **52**, 193–231 (2001). Copyright 2001 Annual Reviews, Inc.[1]

Details can be found in Ref. 1 of the synthesis, physical structure, and electronic structure of quantum films (viz., 1D quantum wells), in specific configurations of single quantum wells, multiple quantum wells with thick potential barriers between the wells to prevent electronic coupling between them, and multiple quantum wells with thin barriers (termed superlattices), which allow electronic coupling (wavefunction overlap) between wells resulting in the creation of delocalized electron density between the wells and quantized miniband formation throughout the 1D superlattice structure. Figure 5 shows the difference in electronic energy level structure between Multiple Quantum Wells (MQWs) and superlattices (SLs).

For high temperature, vapor-phase–grown nanostructures, the critical barrier thickness at which miniband formation in superlattices begins depends upon the effective masses of the tunneling carriers and the barrier height. For a GaAs/$Al_xGa_{1-x}As$ superlattice, the critical barrier thickness is reported to be about 40 Å;[41] the electronic coupling and miniband thickness increases rapidly with decreasing barrier thickness, and miniband formation is very strong below 20 Å[41] (see Fig. 18, and chapter 1 of Ref. 41). Superlattice structures produce efficient charge transport normal to the layers because the charge carriers can move through the minibands via efficient quantum-mechanical

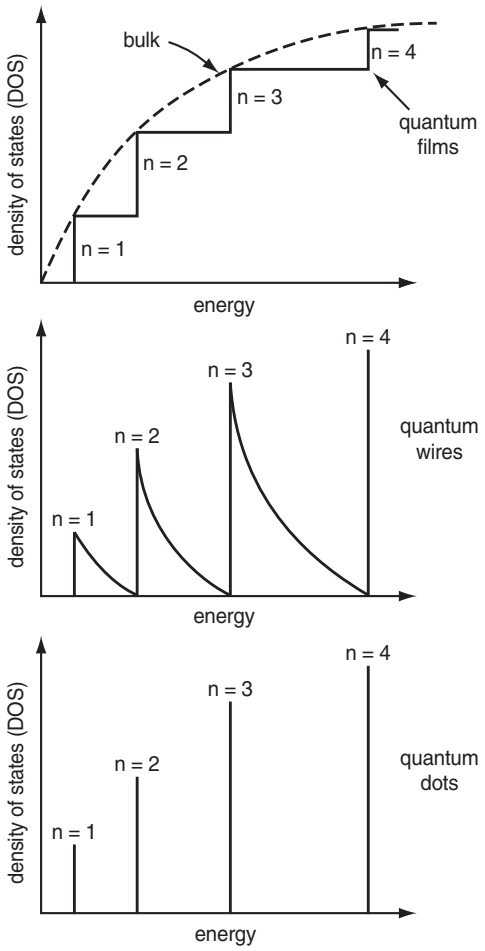

FIG. 4. Density of states depending upon dimensionality of quantum confinement: bulk semiconductors, quantum films, quantum wires, and quantum dots. Reprinted with permission from Nozik and Memming, J. Phys. Chem. **100**(31), 13061–13078 (1996). Copyright 1996 American Chemical Society.[159]

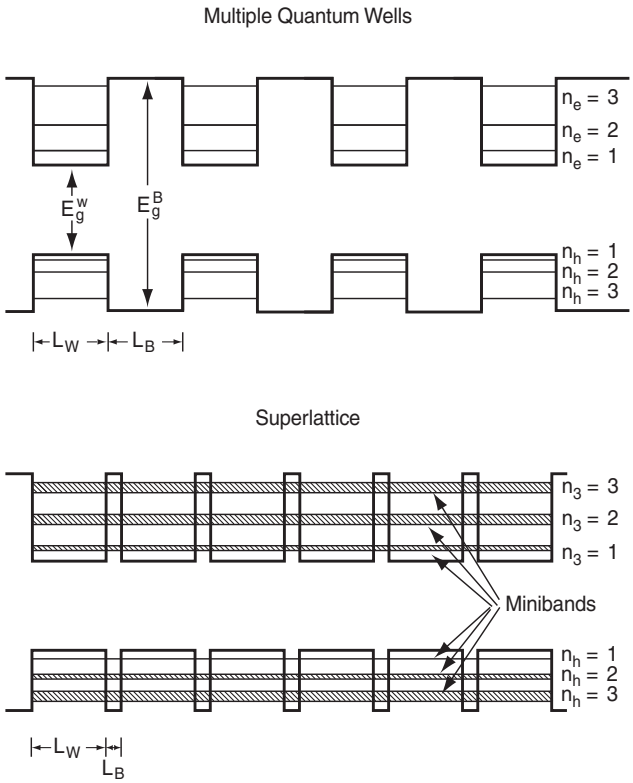

FIG. 5. Difference in confinement of electronic states between multiple quantum well structures (barriers thick enough to prevent carrier tunnelling) and superlattices (barriers thin enough to allow tunnelling); miniband formation occurs in the superlattice structure, which permits carrier delocalization across the nanostructure. Reprinted with permission from Nozik and Memming, J. Phys. Chem. **100**(31), 13061 (1996). Copyright 1996 American Chemical Society.[159]

tunneling; the narrower the barrier, the wider the miniband and the higher the carrier mobility.

Three-dimensional confinement in QDs is usually produced through relatively simple colloidal solution chemistry under ambient or moderate temperatures; this is a great advantage of colloidal quantized semiconductor synthesis. Qwires can also be produced via colloidal chemistry.[44] Quantum films formed as colloidal nanocrystals with the dimensions of the flat planar surface in the nanometer range are termed nanoplatelets; depending upon the size and geometric shape of the planar surface, these nanoplatelets may or may not be quantum confined in only 1 dimension, but could be quantum confined in 2–3 additional dimensions. Quantized nanostructures may also be formed via MOCVD and MBE growth techniques; when confined in three dimensions, such QDs are termed Stranski–Krastinov (SK) quantum dots. Further information on the formation of SK dots is presented in Ref. 1.

Thus, there are many 3D geometric forms of nanostructures; if at least one of the 3 dimensions are in the quantum regime (2 to 20 nm), then the nanoparticles are classified as quantized nanoparticles. However, nanoparticles in the nanoscale regime can also be too big to produce quantum effects (i.e., they are bigger than the Bohr radius or de Broglie wavelength of the relevant carriers), but they can still exhibit interesting properties, like slow hot-carrier cooling, that are a consequence of their geometric shape or other unique physical characteristics. For example, for the case of 1D nanostructures with the radial dimension outside the size for quantum effects, the materials are referred to as nanowires or nanorods rather than quantum wires (Qwires).

During the past decade, nanowires have been studied and show interesting effects normally attributed to quantization, including slowed hot-carrier cooling,[45–47] and significant PCEs in nanowire solar cells.[48–51] True quantum wires (Qwires) also exhibit the interesting effects of slow, hot electron cooling and enhanced MEG, but they arise from quantum confinement.[52,53] All these effects will be discussed in the appropriate sections to follow in this review. However, the focus of this review is on quantization effects in quantum films and quantum dots; this is because the volume and extent of this research is presently much greater than for Qwires or nanowires. Thus, the following sections: Secs. I C–I F, II A, II B, IV, V A, V B, VI, and VIII will present much more fundamental background information on QWs, MQWs, superlattices, and QDs. Notwithstanding, Qwires and nanowires are very interesting and

promising nanocrystals that also have a significant potential to impact the basic science and various applications of nanostructures.

C. Energy levels and density of states in quantum wells and superlattices

Discrete energy levels are formed in the quantum wells as electrons or holes are confined by the potential barriers of the well, compared to the continuum of states that exists in bulk material; quantization also leads to a major change in the density of states. The energy levels can be calculated by solving the Schrödinger equation for the well-known 1D "particle in a box" problem using the effective mass envelope function approximation;[41–43,54–58] details are presented in Ref. 1.

For the case where the well is infinitely deep with infinitely high barriers, the solution to the Schrödinger equation becomes simple because the wave functions must be zero at the well-barrier interfaces. In this case, the well-known solution is

$$\Psi = A\sin\frac{n\pi z}{L_w}, \tag{3}$$

$$E_n = \frac{h^2}{2m^*}\left(\frac{n\pi}{L_w}\right)^2, \quad n = 1, 2, 3, \ldots, \tag{4}$$

where L_w is the well width and n is the single principal quantum number. The more realistic case of finite barrier heights and assuming equal effective masses in the well and barrier is also discussed in Ref. 1.

The calculation of hole levels is much more complicated because the band structures of many important semiconductors have hole bands with four-fold degeneracy at $k = 0$. This leads to heavy and light holes with different effective masses. Consequently, in the QW, a double set of hole energy levels is formed with different spacings between levels—one set is for the light holes, the second set is for the heavy holes. Solutions to the problem have been reported for both infinite[43,54] and finite[55,66] potential barriers.[1]

For superlattices, several approaches have been used to calculate the energy level structure of the minibands.[42,57] One approach is to use a tight-binding model for the multiple wells leading to a Bloch-like envelope function.[1]

Profound changes in the density of states [DOS or N(E)] occurs with changes in the dimensionality of quantization (Refs. 57 and 58, and Fig. 4). For ideal bulk semiconductors with simple parabolic energy bands, the DOS has a square root dependence on electron energy[1]

$$N(E)_{Bulk} = \sqrt{2}(m^*)^{3/2}\pi^{-2}h^{-3}E^{1/2}. \tag{5}$$

For an ideal QW film with 1 degree of spatial confinement, the DOS shows a step-like function with each plateau having a DOS of

$$N(E)_{QW} = nm^*/\pi h^2, \tag{6}$$

where n is the quantum number of the state.[1] The steepness of the steps is diminished in a superlattice by the dispersion of the N states in the minibands.[1] For 2D confined quantum wires, the DOS shows a smooth decreasing function between spikes at the principal quantum numbers, while for 3D confined QDs, the DOS show single sharp lines at each principal quantum number, as in a simple ideal atom.

D. Energy levels and density of states in quantum dots

The effective mass approximation (EMA) is the earliest and simplest treatment of the electronic states of a QD; the simple EMA treatment can be improved by incorporating the $\mathbf{k} \cdot \mathbf{p}$ approach that has been commonly used to calculate the electronic structure of bulk semiconductor and QW structures.

The major assumption of the EMA is that if the QD size is larger than the lattice constants of the crystal structure, then the QD will retain the lattice properties of the infinite crystal and have the same values of the carrier effective masses.[1] The QD electronic properties are determined by solving the Schrödinger equation for a particle in 3D confinement. A perfectly spherical QD with infinite potential walls at the surface is a proper zeroth order approximation.

Perturbation theory[59,60] leads to a solution of the form

$$E_{\min} = \frac{h^2\pi^2}{2R^2}\left[\frac{1}{m_e^*} + \frac{1}{m_h^*}\right] - \frac{1.8e^2}{\varepsilon R} - 0.25E_{Ryd}^*, \tag{7}$$

where $E_{\min}$ is the lowest energy separation between hole and electron states, E_{Ryd}^* is the bulk exciton binding energy in meV, and R is the QD radius. Even though there are no bands in a quantized nanocrystal, $E_{\min}$ is often simply referred to as the bandgap of the QD because it represents the threshold energy for photon absorption, blue-shifted from the bulk bandgap, E_g.

For 3D spatial confinement in QDs, the solution of the Schrödinger equation creates electronic states described by three quantum numbers plus spin. A commonly used notation[1] labels the electron states as nLe and the hole states as nLF, where n is the principal quantum number (1, 2, 3, etc.), L is the orbital angular momentum (S, P, D, etc.), and F is the total angular momentum (F = L + J and J = L + S), where S is the spin, and the projection of F along a magnetic axis is mF = – F to + F. Thus, electron states become 1Se, 2Se, 1Pe, etc., and hole states become $1S_{1/2}$, $1S_{3/2}$, and $1P_{1/2}$, etc. For optical interband transitions between quantized hole and electron states in ideal spherical QDs, the selection rules are $\Delta n = 0$, $\Delta L = 0, \pm 2$; and $\Delta F = 0, \pm 1$. These ideal selection rules can be broken by non-spherical QDs and strong hole-state mixing.[1]

E. Optical spectroscopy of 1D quantum wells and superlattices

Optical transitions between quantum levels occur upon excitation with light. The interband transition probability is the product of an optical matrix element (M) times a DOS. M is the electric dipole operator and can be written as[1,58]

$$\mathrm{M} = \left(\varphi_e(z)e^{ike\bullet r}U_{cke}(r)|\eta|\varphi_h(z)e^{ikh\bullet r}U_{vkh}(r)\right), \tag{8}$$

where $\varphi_e(z)$ and $\varphi_h(z)$ are the electron and hole envelope wave functions, k_e and k_h are electron and hole wave vectors, η is the polarization vector of the light, and $U_{vkh}(r)$ are the Bloch functions. Based on Eq. (8), the selection rule for optical interband transitions is that $\Delta n = 0$, where n is the quantum number of the energy level in the well. Some additional factors affecting optical transitions are described in Ref. 1.

Thus, the optical absorption spectrum of a quantum film consists of a series of steps, with the energy position of these steps corresponding to the transitions between heavy or light hole–quantum states and

electron quantum states following the above selection rule $\Delta n = 0$. Furthermore, the exciton binding energy is greatly increased in QWs because the widths of the wells are commonly smaller than the diameter of an exciton and the excitons can thus be stable even at room temperature. Therefore, unlike bulk semiconductors, the absorption spectra of QWs can show exciton peaks at room temperature which occur at energies below that of the energy step. Such spectra have indeed been observed by many researchers.[41–43,54–58]

F. Optical spectroscopy of quantum dots

QDs exhibit the same general optical absorption and emission photophysical properties as QWs and SLs; the probability for dipole-allowed optical transitions is proportional to the following matrix element connecting the initial [$\Psi_i(r)$] and final [$\Psi_f(r)$] states through the dipole operator ($\boldsymbol{\eta}$):

$$M_{QD} = \langle \Psi_f(r) | \hat{\boldsymbol{\eta}} | \Psi_i(r) \rangle. \tag{9}$$

The wave functions for 3D confinement have three quantum numbers (n, l, m) plus spin, and for interband transitions, the selection rules for dipole-allowed absorption and emission are $\Delta n = 0$. For intraband transitions between the ladder of electron or hole states, the selection rules for the simplest case of noninteracting electrons and holes are $\Delta n \neq 0$; $\Delta L = 0, \pm 1$; and $\Delta m = 0, \pm 1$.

The room-temperature absorption and emission spectra as a function of indium phosphide (InP) QD sizes ranging from 26 to 60 Å [measured by transmission electron microscopy (TEM)] are shown in Ref. 61; the exciton energy for emission spectra was 2.48 eV. The absorption exhibits one or more broad excitonic peaks which reflect substantial inhomogeneous line broadening arising from the QD size distribution; as expected, the spectra shift to higher energy as the QD size decreases.[61] Bulk InP is black having an absorption onset at 918 nm which relates to a room-temperature bandgap of 1.35 eV. Higher energy transitions above the first excitonic peak in the absorption spectra can also be easily seen in QD samples with mean diameters equal to or greater than 3 nm. The global emission peaks show an increasing red shift up to a maximum of 300 meV at 26 Å. caused by the dominance of the larger particles in the size distribution.[61]

II. HOT-CARRIER RELAXATION DYNAMICS IN QUANTIZED AND NON-QUANTIZED SEMICONDUCTORS

A. Hot electron cooling dynamics in quantum wells and superlattices

Studying hot-electron cooling dynamics is very critical for understanding the creation of hot-carrier effects; the slower the hot-carrier cooling, the more likely will the beneficial effects be realized of hot-carrier photoconversion to electricity and solar fuels. Several types of time-resolved photoluminescence (PL) experiments can produce very useful information about hot-carrier cooling dynamics. Hot luminescence nonlinear correlation[1,62–64] measurements is one such technique. As an example, in Fig. 2 of Ref. 52, the hot-electron relaxation times as a function of the electron energy level in the 1D quantized well regions are shown for a 20-period MQW of GaAs/$Al_{0.38}Ga_{0.62}As$ containing 250 Å GaAs wells and 250 Å $Al_{0.38}Ga_{0.6}$ As barriers, compared to the energy level above the bandgap for bulk GaAs. For bulk GaAs, the hot-electron relaxation time varies from about 5 ps at the highest excitation energy to 35 ps near the bottom of the conduction band. For the MQW, the corresponding hot-electron relaxation times are 40 ps and 350 ps for the same excess photon energy above the bandgap.

Another technique to measure PL lifetimes of hot electrons involves using time-correlated single photon counting.[33] For example, Fig. 1 from Ref. 33 (shown here in Fig. 6) shows 3D plots of PL intensity as a function of energy and time for bulk GaAs and a 250 Å GaAs/250 Å° $Al_{0.38}Ga_{0.62}As$ MQW.[1,33] These plots clearly show that MQWs exhibit much longer-lived hot luminescence (i.e., luminescence above the lowest $n = 1$ electron to heavy-hole transition at 1.565 eV) compared to bulk GaAs. The hot PL for the MQW exhibits longer lifetimes that range from hundreds to several thousand ps. On the other hand, hot PL emission above the bandgap (1.514 eV) for bulk GaAs is negligible over most of these photon energy and time regimes.

The cooling (energy–loss) rate for hot electrons is determined by longitudinal optical (LO) phonon emission through electron-LO-phonon interactions. The time constant characterizing this process can be described by the following expression:[1,65–67]

$$P_e = -\frac{dE}{dt} = \frac{h\omega_{LO}}{\tau_{avg}} \exp\left(-h\omega_{LO}/kT_e\right), \tag{10}$$

where Pe is the power loss of electrons (i.e., the energy-loss rate), $h\omega_{LO}$ is the LO phonon energy (36 meV in GaAs), T_e is the electron temperature, and τ_{avg} is the time constant characterizing the energy-loss rate.

The results of calculations determining τ_{avg} as a function of electron temperature[1,33] from Eq. (10) is shown in Fig. 2 of Ref. 33 for bulk and MQW GaAs at high and low carrier densities. The τ_{avg} values at a high carrier density [$n_c \sim (2-4) \times 10^{18}$ cm^{-3}] for the MQW are much higher ($\tau_{avg} = 350$–550 ps for T_e between 440 and 400 K), compared to bulk GaAs ($\tau_{avg} =$ 10–15 ps over the same T_e interval). Alternatively, at a low carrier density [$n_c \sim$ (3–5) 10^{17} cm^{-3}], the differences between the τ_{avg} values for bulk and MQW GaAs are minor.

A third technique to measure cooling dynamics is PL upconversion.[1,33] In Ref. 33, time-resolved luminescence spectra were recorded at room temperature for a 4000-Å bulk GaAs sample at the incident pump powers of 25, 12.5, and 5 mW. The electron temperatures were determined by fitting the high-energy tails of the spectra; The carrier densities for the sample were 1×10^{19}, 5×10^{18}, and 2×10^{18} cm^{-3}, corresponding to the incident excitation powers of 25, 12.5, and 5 mW, respectively. Similarly, spectra for the MQW sample were recorded at the same pump powers as the bulk. Figure 6 presents the τ_{avg} for bulk and MQW GaAs at the three light intensities, again showing the much slower cooling in MQWs (by up to two orders of magnitude).

Differences in hot-electron relaxation rates between bulk and 1D quantized GaAs structures can also be obtained from time-integrated PL spectra. Typical results are shown in Fig. 7. Here, single photon counting data were taken with 13 ps pulses of 600 nm light at 800 kHz focused to an average power of 25 mW.[1] Fitting the tails of these PL spectra to the Boltzmann function produced time-averaged electron temperatures that varied from 860 K for the 250 Å/250 Å MQW to 650 K for the 250 Å/17-Å superlattice, whereas bulk GaAs had an electron temperature of 94 K, close to the lattice temperature of 77 K.

Thus, much data from many independent studies using different spectroscopic techniques show that hot-carrier cooling rates depend upon photogenerated carrier density; the higher the electron density, the slower the cooling rate. Furthermore, this effect is most pronounced for quantized nanostructures, but is also found in bulk GaAs,

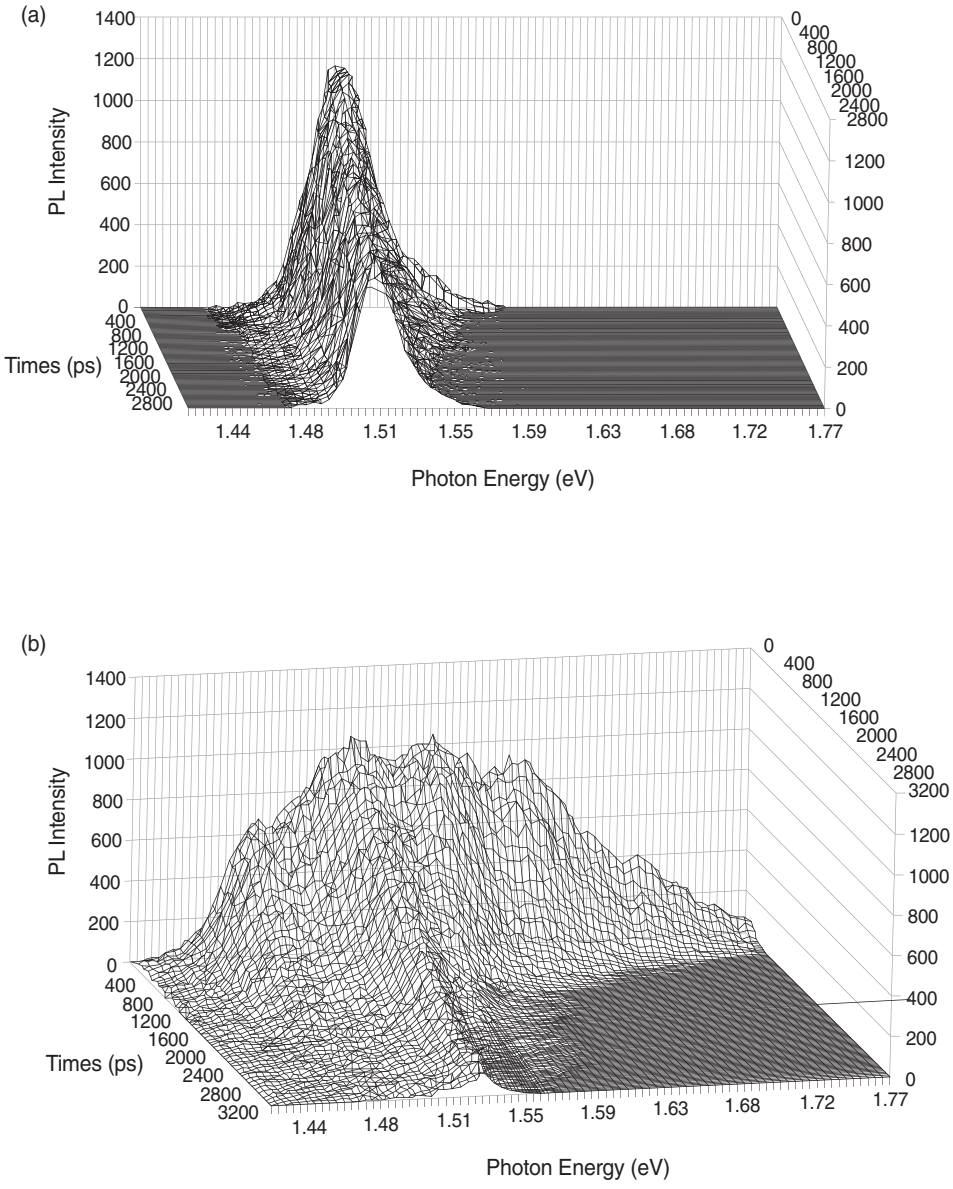

FIG. 6. Three-dimensional plots of photoluminescence intensity vs time and photon energy for (a) bulk GaAs and (b) 250 ÅGaAs/250 Å $Al_{0.38}Ga_{0.62}As$ MQW. The MQW nanostructure exhibits a hot luminescence tail from hot-carrier radiative emission. Reprinted with permission from Rosenwaks *et al.*, from Phys. Rev. B **48**, 14675 (1993) Copyright 1993 American Physical Society.[43]

but as a much weaker effect. The most generally accepted mechanism for the decreased cooling rates in GaAs QWs is an enhanced "hot-phonon bottleneck"[69–71] (Fig. 8).

In this mechanism, a large population of hot carriers produces a nonequilibrium hot distribution of phonons (in particular, LO phonons that dominate the electron–phonon interactions at high carrier energies); these LO phonons cannot equilibrate fast enough with the crystal bath, and thus, they can be reabsorbed by the electron plasma to keep it hot.

The S-Q type PCE calculation as a function of the hot electron temperature is presented in Fig. 9 in the limit of very slow cooling whereby all hot carriers can be extracted for useful free energy production. In this case, at the earth's surface under AM1.5 solar excitation (see Sec. V A for definition of AM1.5), the electron temperature reaches 3000 K and the theoretical maximum PCE is calculated to be about 66%.

For non-quantized bulk semiconductors, another approach to the study of slowed hot-carrier dynamics is to investigate semiconductors that have large differences between their acoustic and optical phonon energies (such as the Group III-nitrides); when present, the transition of optical phonons into acoustic phonons which couple to the lattice in the last step of carrier cooling, is blocked.[72,73] This approach is another type of phonon bottleneck but does not require the generation of a large density of hot electrons followed by hot phonons. However, the number of semiconductors with the required phonon characteristics that have been studied thus far is rather limited.

A very recent new approach to understanding and realizing slowed cooling and utilization of hot carriers for non-quantized solar

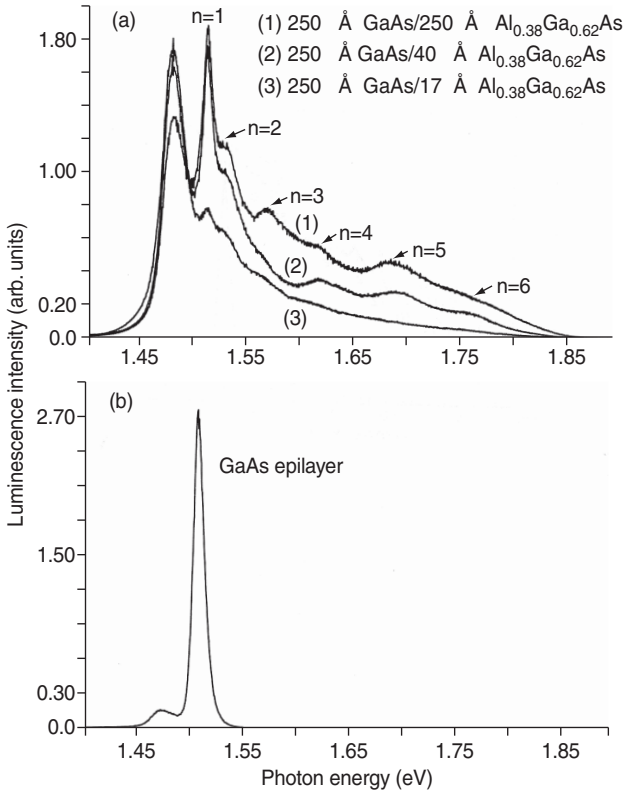

FIG. 7. (a) Time-integrated photoluminescence spectra for multiple quantum wells and SLs showing hot luminescence tails and high energy peaks arising from hot-electron radiative recombination from upper quantum levels. (b) Equivalent spectrum for bulk GaAs showing no hot luminescence. Reprinted with permission from Nozik *et al.*, Solid State Comm. **75**, 297–301 (1990). Copyright 1990 Elsevier.[68]

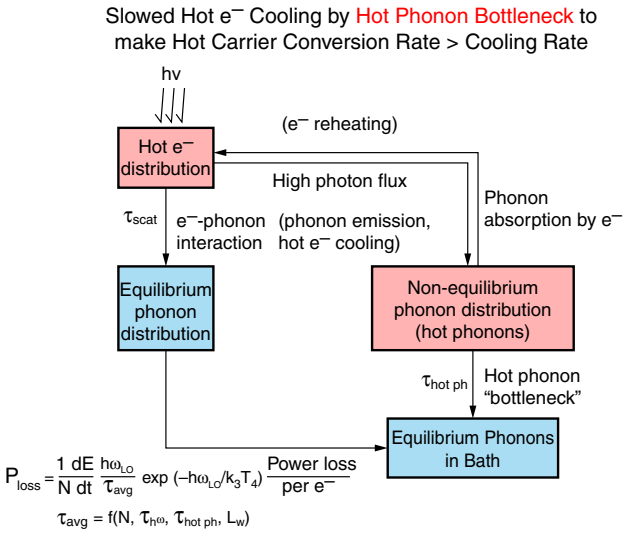

FIG. 8. Mechanism of slowed hot-carrier cooling due to a hot phonon bottleneck created by a high density of hot carriers which create hot phonons that reheat cooling electrons.

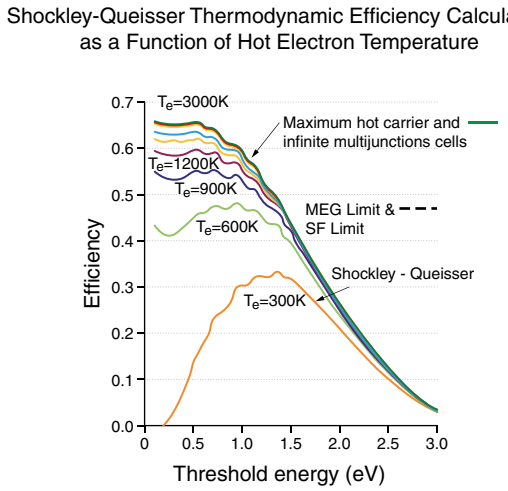

FIG. 9. Shockley–Queisser values of PCE vs E_g for various hot electron temperatures and conventional S–Q calculation assuming complete cooling of hot electrons. Reprinted with permission from Ross and Nozik, J. Appl. Phys. **53**, 3813 (1982). Copyright 1982 American Institute of Publishing.[10]

cells based on bulk semiconductors invokes the role of intervalley scattering from the initially photogenerated and occupied hot carriers in the Γ valley to the upper satellite L and X valleys in III-V semiconductors.[74–77] This approach is termed "valley photovoltaics",[74–77] and initial experimental results[74–77] support this possible route to slow hot-carrier cooling and higher efficiency hot-carrier solar cells.

B. Hot-carrier cooling in semiconductor quantum dots

As discussed and shown previously above, slow hot-electron cooling in QWs and superlattices that is created by a conventional hot phonon bottleneck requires very high light intensities to produce the required high photogenerated carrier density above 1×10^{18} cm^{-3}. This needed intensity can be achieved with laser excitation, but such a level of excitation is greater than that provided by one sun solar irradiation at the Earth's surface. Hence, a conventional hot-phonon bottleneck effect cannot easily produce slowed hot-carrier cooling in semiconductors with 1-sun solar irradiation.[1] However, 3D confinement in quantum dots (QDs) is more favorable for slowing hot-carrier cooling (Fig. 10).

In the quantum dot case, slowed hot-electron cooling occurs because of the large energy difference between discrete quantum states and the need for simultaneous multiphonon–electron scattering; this can occur theoretically even at arbitrarily low light intensity. This effect is simply called a phonon bottleneck, without the need for high light intensity and the creation of hot phonons. Thus, as discussed previously, slowed hot-carrier cooling in QDs can increase the possibility of carrier multiplication [termed multiple exciton generation (MEG) in QDS] through an inverse Auger process[1,12–34] (Fig. 10).

1. Phonon bottleneck and slowed hot-electron cooling in quantum dots

The first prediction of slowed cooling at low light intensities in quantized structures was made by Boudreaux *et al.*[1,11] They

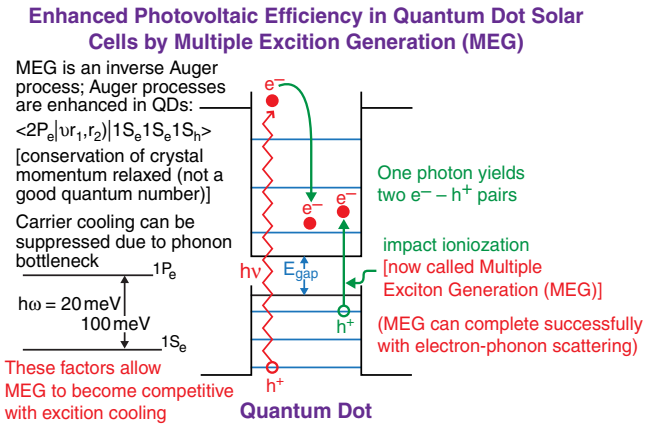

FIG. 10. Quantization in semiconductor quantum dots showing multiple exciton generation (MEG) when absorbed photon energy is $\geq 2E_g$. Two electron-hole pairs are formed from 1 photon with an energy $\geq 2E_g$, and the electron-hole pair exists as an exciton because they are squeezed together by the quantum confinement. Reprinted with permission from Nozik, Physica **E14**, 115–120 (2002). Copyright 2002 Elsevier B. V.[12]

anticipated that cooling of carriers would require simultaneous multiphonon–electron scattering, which is much less probable when the quantized levels are separated in energy by much more than a single phonon energy. They analyzed the expected slowed cooling time for hot holes in the depletion layer of highly doped n-type TiO_2 semiconductors, wherein quantized energy levels arise because of the narrow depletion layer produced by the high doping level. For example, at a doping level of 1×10^{19} cm^{-3}, the potential well in this space charge layer can be approximated as a triangular well with its top extending 200 Å from the semiconductor bulk to the surface and with a depth of 1 eV at the surface barrier. The carrier cooling time in this depletion layer was estimated from

$$\tau_c \sim \omega^{-1} \exp(\Delta E/kT), \tag{11}$$

where τ_c is the hot-carrier cooling time, ω is the phonon frequency, and ΔE is the energy separation between quantized levels.[1,11] For strongly quantized electron levels, with $\Delta E > 0.2$ eV, τ_c is greater than 100 ps according to Eq. (11).[1,11]

In heavily doped semiconductors, carriers present in the space charge (i.e., depletion) layer at the surface are only confined in one dimension, as in a quantum film. This quantization regime produces energy states that have dispersion in k-space.[1] Thus, hot carriers can cool by undergoing interstate transitions that require only one emitted phonon per electron–phonon scattering event, followed by a cascade of single phonon–electron intrastate scattering interactions. The lowest energy level of each quantum state in the depletion layer is reached by sequential intrastate relaxation events before the final interstate transition occurs to the lowest state level. Therefore, the simultaneous and slow multiphonon–single electron relaxation pathway can be bypassed by single phonon–electron scattering events, and the cooling rate increases correspondingly.[1]

Advanced theoretical models have been proposed by Bockelmann and co-workers[78,79] and Benisty and co-workers.[80,81] for slowed cooling in QDs. This mechanism[80,81] for slowed hot-carrier cooling and a phonon bottleneck in QDs depends upon hot-carrier cooling occurring only via longitudinal optical (LO) phonon emission. However, several other mechanisms exist by which hot electrons can cool in QDs. The most prominent among them is the Auger mechanism[82] discussed previously. In this mechanism, the excess energy of the electron is transferred via an Auger process to the hole, exciting it to higher energy, and the excited hole then cools rapidly because of its larger effective mass and smaller energy-level spacing in the quantum well occupied by holes. Thus, such an Auger mechanism for hot-electron cooling can break the phonon bottleneck.[82] Other possible mechanisms for breaking the phonon bottleneck are: electron-hole scattering,[83] deep-level trapping,[84] and acoustical–optical phonon interactions.[85,86]

2. Experimental determination of the cooling dynamics and phonon bottlenecks in quantum dots

In prior years, many studies have been published that explore hot-electron cooling/relaxation dynamics in III-V QDs and the issue of a phonon bottleneck in QDs.[1,87] The results are controversial and there are many reports that both support[88–102] and contradict[103–115] the prediction of slowed hot-electron cooling in QDs and the existence of a phonon bottleneck.[1] Some reports claiming an absence a phonon bottleneck do so because the time of cooling was not sufficiently long enough (i.e., > several ps) to qualify as slow cooling. However, in the context of hot electron extraction for useful work, it has been shown in Refs. 116–118 that the electron transfer times at semiconductor–molecule interfaces can be sub-ps to a few ps, and hence, hot electron cooling times of 5 to 10 ps would be sufficiently long for hot electron transfer to occur, especially in the context of solar fuels production.

In addition to studies on slowed carrier cooling conducted on SK-type III-V QDs, studies of carrier cooling and relaxation have also been performed on II-VI CdSe colloidal QDs by Klimov *et al.*[1,108,110–121] and Guyot-Sionnest *et al.*;[1,88] the results are discussed in Ref. 1. These studies support the Auger mechanism for hot-carrier cooling, whereby the excess energy of the hot carrier is rapidly transferred to the lowest energy carrier of the opposite sign that has a higher density of states (DOS), which then relaxes rapidly through its higher DOS. Thus, for example, when a cold photogenerated hole is rapidly removed and trapped at the QD surface, the Auger mechanism for hot electron relaxation becomes inhibited and the hot electron relaxation rate slows. Other dynamical studies of hot-carrier relaxation also strongly support an Auger mechanism for relaxation process in QDs (reviewed in Ref. 1).

It is noted that the same QD systems studied by different researchers using different spectroscopic techniques also showed both slowed cooling and fast cooling when different experimental techniques were used. This suggests a strong sample-history dependence[122,123] for the results; for example, the samples could have differences in their defect concentration and type, surface chemistry, morphology, and other physical parameters that affect carrier cooling dynamics.[1] Additional research is required to sort out these contradictory results.

3. Slow hot-carrier cooling in non-quantized nanowires and enhanced MEG in quantized Qwires

Recent studies[45–47] of slow hot-carrier relaxation in nanowires of various III-V semiconductor materials and structures (InP, GaAS, and

heterowires of GaAs/InP and InP WZ-ZB), demonstrated significant slowed cooling; the diameters of the nanowires in these studies are not in the quantum-confined regime and the slowed cooling is therefore not due to quantization effects, but rather to unique properties of the nanowire structures. Experiments with 70 nm diameter nanowires of GaAs and InP showed the formation of carrier temperatures of 500 K with a lattice temperature of 310 K with cw excitation and effective hot-carrier lifetimes of up to 1 ns.[45] Studies of Type II heterojunctions of wurtzite/zinc-blend nanowires of InP showed slowed hot-carrier cooling that was attributed to a high density of stacking faults in the nanowires;[46] the lifetimes of hot carriers in this system was estimated to be 10s of ps. In nanowire core-shell heterojunctions with 70 nm $GaAs_{0.7}Sb_{0.3}$ cores and 30 nm InP shells, hot-carrier lifetimes of several 100s of ps were determined using transient Rayleigh scattering at 10 K.[47]

Regarding quantization effects in 1D structures, enhanced MEG (multiple exciton generation) has also been observed in quantized 4.4 nm quantum wires (Qwires) of PbSe.[52,53] The enhanced effects was a decrease of the threshold photon energy for the onset of MEG from a value of 2.7 for PbSe QDs to 2.21 times the bandgap of quantized PbSe Qwires.[52] The theoretical PCE for MEG-based solar photoconversion is maximized when the threshold energy is 2.0 times the bandgap of the quantized nanostructure,[16] so the PbSe Qwires will have theoretical PCEs greater than bulk PbSe or QDs of PbSe.

III. SLOW COOLING OF HOT CARRIERS IN NON-QUANTIZED BULK SEMICONDUCTORS

A. Bulk semiconductors with wide phononic gaps and valley photovoltaics

For non-quantized bulk semiconductors another approach to the study of slowed hot-carrier dynamics is to investigate semiconductors that have large differences between their acoustic and optical phonon energies (such as the Group III-nitrides); these materials are described as having wide phononic bandgaps. In this case, the transition of optical phonons into acoustic phonons, which couple to the lattice in the last step of carrier cooling, is blocked.[72,73] This approach is another type of phonon bottleneck but does not require the generation of a large density of hot electrons followed by hot phonons. However, the number of semiconductors with the required phonon characteristics that have been studied thus far is rather limited.

A very recent new approach to understanding and realizing slowed cooling and utilization of hot carriers for non-quantized solar cells based on bulk semiconductors invokes the role of intervalley scattering from the initially photogenerated and occupied hot carriers in the Γ valley to the upper satellite L and X valleys in III-V semiconductors.[74–77] This approach is termed "valley photovoltaics",[74–77] and initial experimental results[74–77] support this possible route to slow hot-carrier cooling and higher efficiency hot-carrier solar cells.

B. Non-quantized perovskites

Perovskite materials [general formula ABX_3, where A = cation 1, B = cation 2 (frequently a metal), and X = a halide (or oxygen)] and their crystal structures (where cation A is in a cubo-octahedral cage formed by the 12 nearest neighboring X anions, cation B is octahedrally surrounded by six X anions have been known for greater than 100 years. However, only over the past decade have some perovskite compositions been recognized as excellent materials for producing highly efficient, high photovoltage, and low cost photovoltaic solar cells,[35–40,124,125] and they are shown in Table 1. The initial perovskite composition that initiated the intense study of perovskites for solar cells was $(CH_3NH_4PbI_3$ (MAPbI); the early work began using MAPbI as a sensitizer in a dye-sensitized photoelectrochemical cell,[124] followed by MAPbI nanocrystals deposited on films of TiO_2,[125,126] to a mixed halide nanocomposite architecture of MAPbI and on Al_2O_3,[127] and finally to a planar perovskite p-n structure [128–130]

TABLE I. Perovskite molecules studied for slow, hot-carrier cooling.

$CH_3NH_3PbI_3$ films
$CH_3NH_3PbI_3$ nanowires
$HC(NH_2)(NH_2)Pbl_3$ films
$HC(NH_2)(NH_2)Snl_3$ nanocrystals (t_{cool} = 1 ns)
$CsPbBr_3$ single crystals
$CH_3NH_3Snl_3$
$Cs_2Til_yBr_{6-y}$ (y = 0, 2, 6)
$CsPbX_3$ (X = Br, l) nanocrystals
CH_3Sbl_3 nanocrystals
$(CH_3(CH_2)_8NH_3)_2(CH_3NH_3)_{n-1}$ Pb_nX_{3n+1}), X = Br^-, l^-, (n = 1, 2), "natural" MQWs (inorganic layer = well; organic layer = barrier), (t_{cool} = 1 ns)

Since 2009, the total number of published papers on perovskites has skyrocketed from one in 2009 to >56 000 in 2020. The record PCE of perovskite-based single junction laboratory solar PV cells has reached about 26% in 10 years, to be compared to crystalline silicon cells at 26.1% after 65 years of research and development (R&D). Perovskites do have problems with photostability and the toxicity of some elements (e.g., Pb) in some perovskite compositions, but their high PCE and low-cost processing to produce low-cost energy production make perovskites an attractive future candidate for very-low- cost PV cells if their potential toxicity can be ameliorated or safely accommodated.[131–140]

A very interesting discovery for perovskites films is that they are reported to exhibit remarkably slow cooling of hot carriers, both through a hot phonon bottleneck created with high photoexcitation intensity and without high intensity photoexcitation;[141–145] Table I lists 10 molecules that have been recently studied and showed slowed hot-carrier cooling. Some results show exceedingly slow hot-carrier cooling time while other reports show much faster cooling rates. This is similar to the situation previously reported above in Sec. II B 2 for 1D III-V superlattices and quantum well films, as well as for QDs. One attractive proposed reason for the slow hot-carrier cooling in perovskites is the rapid formation of polarons that screen the carriers from electron-LO phonon interactions, thus inhibiting this normally fast cooling mechanism.[145]

An additional very interesting feature of the electronic structure of perovskites is that the effective masses of electrons and holes are frequently low but comparable, unlike conventional inorganic semiconductors used for solar photoconversion where the hole effective mass is usually much heavier than that of the electron. This causes some degree of contention and controversy about the mechanism of slow hot-carrier cooling in perovskites and the roles of hot electrons vs hot holes and/or their combined effects and interactions.[146]

The first indication of slow hot-carrier cooling due to a hot phonon bottleneck in photoexcited perovskites was made in 2016.[141] Since

2016 through late 2020, more than 350 papers have been published on the topic of slow hot-carrier cooling in perovskites; this work includes many reviews. This specific topic is being researched very heavily and intensely, and thus, it is suggested interested readers should conduct a literature search under the subject "hot-carrier cooling in perovskites" to access the latest progress and reviews on this interesting and important relatively new topic.

IV. MEG ANALOGY: CARRIER MULTIPLICATION THROUGH SINGLET FISSION IN MOLECULES

In 2004, Nozik *et al.* suggested[147] that a molecular analog to MEG was possible in certain molecular chromophores where the triplet state is $\sim^1/_2$ the energy difference between the singlet ground state and 1st excited state (S_0 – S_1); a process termed singlet fission (SF)[16,35–40,124–126] Singlet fission, the conversion of one singlet exciton to two independent triplet excitons, in an organic molecular chromophore, was discovered and its fundamentals were elucidated in the 1960s.[36] It is only efficient in materials in which the excitation energy to the lowest excited singlet is about twice that to the lowest triplet. Such organic chromophores are relatively rare. Figure 11 shows 24 molecular chromophores that exhibit SF.[39]

In 2006, a seminal paper by Hanna and Nozik[16] analyzed the PCE values of SF solar cells quantitatively and pointed out that a combination of a singlet-fission solar material absorbing higher-energy solar photons and ordinary solar material for lower-energy photons in optical series but electrically in parallel is free of any requirements for current matching and is capable of substantially beating the Shockley–Queisser limit of 33% by generating a maximum theoretical efficiency of ∼46%. In the same year, Paci *et al.* and Smith and Michl pointed out that two classes of chromophores, bi-radicaloids and large aromatic hydrocarbons, provide likely candidates for efficient SF materials and used quantum chemical calculations to produce a long list of candidates.[35,36] In 2009–2010, five independent groups of investigators reported fully efficient SF (100% QY for SF or 200% for total QY);[35–40,148–153] 100% QY for SF was reported for a molecule never previously examined but suggested by theory as possible.[35] These developments, and the availability of a comprehensive review by Smith and Michl published in 2010,[36] attracted attention and in the last 10 years, hundreds of experimental and theoretical papers on the subject have appeared. Much of this work focused on investigation of the mechanism of SF in polyacenes, a group of compounds in which it was initially discovered, and their derivatives. Much new photophysics emerged from this effort. Initially, only a handful of truly efficient materials was known, and few, if any of those, appeared practical. This is now beginning to change as theoretical guidelines for the design of chromophore structure and packing emerge. The development and testing of these guidelines is underway; these efforts are summarized in several reviews.[148–153]

V. CONVERSION OF PHOTOGENERATED HOT CARRIERS INTO ADDITIONAL FREE ENERGY TO ENHANCE THE POWER CONVERSION EFFICIENCY OF SOLAR CELLS

A. Utilizing hot carriers in bulk semiconductors for enhanced power conversion efficiency

Hot-carrier transfer in the context of potentially more efficient solar photon conversion to solar fuels was first introduced[8–11] from 1978 to 1983, initially demonstrating the supra-band edge reduction of electron-accepting redox reactions at semiconductor-molecule interfaces (in photoelectrochemical cells). However, many studies of hot electron or hot hole charge transfer from the 1990s to 2000s showed only small hot-carrier effects in solar cells for both PV and solar fuels. In 1997, a theoretical study of multiple quantum wells in a photovoltaic p-i-n cell configuration consisting of an i-superlattice containing 25 nm GaAs 1D confined quantum well films sandwiched between thin 1.7 nm n^+ and p^+ $GaInP_2$ barriers indicated the photogeneration of hot electrons with a peak temperature of 2300 K in the superlattice miniband region based on laser excitation.[34] However, experimental studies of this system in a p-i-n cell configuration under illumination, that created a photogenerated forward bias produced by the illumination, resulted in total cooling of hot electrons from the ohmic contacts of the cell that were back-injected into the superlattice region and subsequently quenched the hot electrons in the superlattice i-region, resulting in no increase in PCE.[34] However in a recent paper, Nguyen *et al.* [154] created a single 8 nm quantum well [$In_{0.78}Ga_{0.22}As_{0.81}P_{0.19}$ (Eg = 0.78)] with 130 nm barriers [$In_{0.8}Ga_{0.2}As_{0.435}P_{0.565}$ (Eg = 1.05 eV)]. These authors conducted detailed and rigorous studies of the optoelectronic properties of their cell structure and careful analyses of the data determined thermodynamic properties such as hot electron temperatures (up to 1300 K in the well) and electrochemical potentials. Their analyses confirmed that higher photovoltages and higher photocurrents were generated in their p^+ - i - n^+ PV cell in which a quantum well was imbedded in the i region, compared to the expected cell values if all photogenerated carriers cooled to the lattice temperature. Thus, the extra photocurrent and photovoltage were attributed to the effect of hot carriers created and present in the quantum well. Although the increase in cell performance was small since only one quantum well was present, the results and conclusions are important because they confirm that hot-carrier effects can indeed enhance the PCE of solar cells.

The classic paper[4] of Shockley–Queisser (S–Q) in 1961 showed that the maximum possible power conversion efficiency (PCE), assuming no hot electron effects, was 33% (Fig. 9) for a single bandgap semiconductor PV cell with the sun at a zenith angle of 48.2° (i.e., the angle with respect to the sun's vertical position at high noon that is directly perpendicular to the earth's surface); this produces a solar flux and spectrum that results from the sun's radiation passing through 1.5 atmospheres and the resulting solar spectrum is labeled Airmass 1.5 (AM1.5) (Fig. 9). At the top of the atmosphere, the solar spectrum is labeled AM0; and when the sun is at high noon and passes through 1 atmosphere, the spectrum is labeled AM1. The S–Q limit is calculated at AM1.5 and essentially all terrestrial PV cells are rated at AM1.5. In the S–Q analysis, all hot electrons are assumed to relax to the semiconductor band edges, and the maximum photopotential is therefore the semiconductor bandgap (Eg) minus the entropy loss due to converting solar irradiance into electrical free energy. This intrinsic loss depends upon the bandgap but ranges from about 0.3 eV for optimum bandgaps for PV (1.2 to 1.4 eV) to 0.2 eV for smaller bandgaps. The Ross and Nozik 1982 paper[10] showed that the maximum PCE value for hot-carrier PV cells is the same (Fig. 9) as that approached by a large number of multiple semiconductor homojunctions with different bandgaps that are stacked in a tandem structure and thus connected in series both optically and electrically; the latter system is the one presently used to increase the efficiency of PV cells but it works best

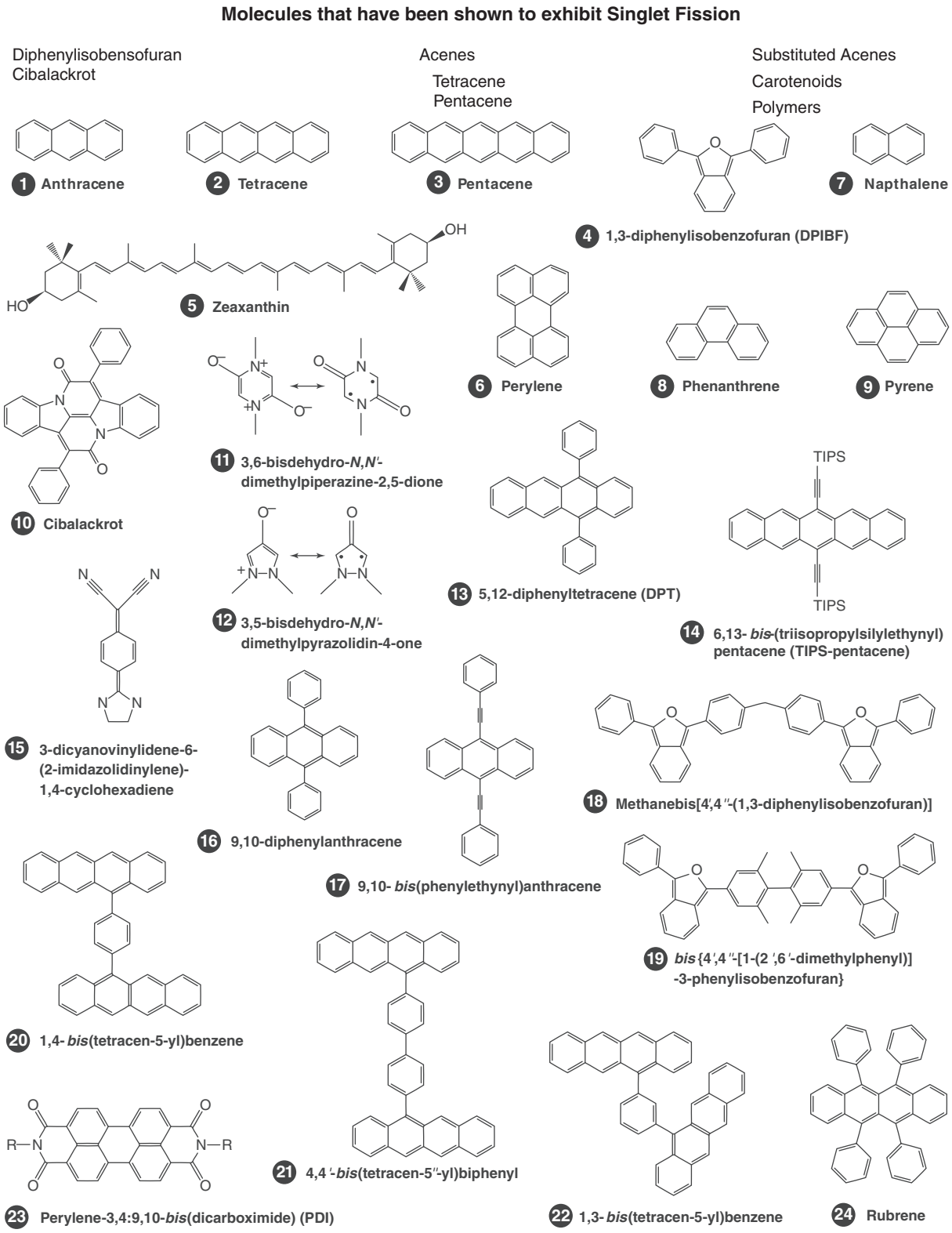

FIG. 11. Singlet fission molecules. Reprinted with permission from Smith and Michl, Annu. Rev. Phys. Chem. **64**, 361–386 (2013). Copyright 2013 Annual Reviews, Inc.[39]

for Group III-V semiconductors and is very expensive. For tandem PV cells with two optimum bandgaps (1.63 and 0.96 eV), the PCE is 47%; for three bandgaps it is 52%; for five it is 58%; and in the limit of an infinite number of bandgaps perfectly matched to the solar spectrum, it is 66%.

As previously discussed, the realization of hot-carrier effects in PV cells is challenging because the carrier cooling rates are usually much faster than the charge transport/transfer rates through the bulk semiconductor and across the cell contacts. However, as also previously discussed above, hot-carrier cooling rates could be slowed in quantized semiconductors to the extent that would make hot charge transport/transfer out of a solar cell (both for PV and solar fuels) or the generation of multiple carriers via MEG, competitive with cooling.

In 2007, several research groups began studies and have reported on the research and development of hot-carrier solar cells based on hot-carrier extraction. Many possible approaches to achieving hot-carrier extraction and utilization before carrier cooling and lattice heating were examined. Recent reviews by D. K. Ferry *et al.*[77] and G. Conibeer *et al.*[72] have reported on these efforts. These reviews[72,77] cover the work of Conniber, Green, Guillemoles, Ekins-Daukes, Le Bris, Lombez, Dimmock, and Sellers. Furthermore, a literature search under the key words "hot carrier solar cells," will provide many additional details of this extensive research topic. Key topics covered by these reviews and literature searches include: (a) creating a phonon bottleneck at one sun light intensity and creating a hot phonon bottleneck with high light intensity that generates high photogenerated carrier density; (b) the use of quantization effects in quantum-confined semiconductors to slow hot-carrier cooling, thus allowing MEG and hot- carrier extraction; (c) exploring bulk semiconductor materials like InN and its analogs, such as II-IV-nitrides, large-mass anion III–Vs, and Group IV alloys, which have large energy gaps between optical phonon energies and lower energy phonons (i.e., they have a phonon bandgap) which can inhibit the Klemens decay, whereby the optical phonons emitted by hot carriers are inhibited from decaying further into lower-energy acoustic phonons that subsequently heat the lattice; and (d) the introduction of Valley Photovoltaics.

The first thermodynamic calculations on ideal, fully hot-carrier solar cells that attain a carrier temperature of 3000 K (Fig. 9) showed they can theoretically achieve the same high conversion efficiency (66%) produced by a large (>6) tandem stack of different ideal bandgaps. As previously stated in Sec. I A, one way to do this is to transport the hot carriers to selective contacts with appropriate work functions and energy transporting windows that only permit hot-carrier removal, followed by injection of the hot carriers into either an electrolyte redox system in a photoelectrochemical fuel-producing cell or through energy-selective contacts in PV cells, before the carriers cool. A second approach (discussed below in Sec. V B) to beneficial hot-carrier utilization is to use the excess kinetic energy of the hot carriers to produce additional electron-hole pairs; however, this approach results in a lower ultimate PCE compared to complete hot-carrier extraction because the threshold photon energy for this effect is twice the value of the semiconductor bandgap in order to conserve energy, and thus, excess photon energy between 1 and 2 times the bandgap is lost as heat. In bulk semiconductors this carrier multiplication process is called impact ionization and is an inverse Auger type of process. However, impact ionization (I.I.) cannot contribute to significantly improved power conversion efficiency in present solar cells based on bulk Si, CdTe, $CuIn_xGa_{(1-x)}Se_2$, or III-V semiconductors because their bandgaps are relatively large and thus, I.I. above $2E_g$ requires blue or UV photons which comprise too small a fraction of the solar spectrum to affect the PCE. Furthermore, in bulk semiconductors, the crystal momentum (**k**) must also be conserved, and this leads to the requirement that the threshold photon energy for I.I. must exceed that needed to only satisfy energy conservation. Additionally, the rate of I.I. must compete with the very fast rate of energy relaxation by phonon emission through electron–phonon scattering. It has been shown that the rate of I.I. in bulk semiconductors becomes competitive with phonon-scattering rates only when the kinetic energy of the photogenerated hot electron is many multiples of the bandgap energy (E_g). In bulk semiconductors, the observed transition between inefficient and efficient I.I. also occurs slowly; for example, in Si, the I.I. quantum efficiency was found to be only 5% (i.e., total quantum yield = 105%) at $h\nu \approx 4$ eV ($3.6 \times E_g$), and 25% at $h\nu \approx 4.8$ eV ($4.4 \times E_g$).

B. Quantum dot solar cells based on the generation of multiple electron-hole pairs (excitons) from hot carriers

Because of spatial confinement (Fig. 10) of electrons and holes in quantum dots, the following effects are present:[1] the e^-h^+ pairs are correlated and thus exist as excitons rather than free carriers;[2] the rate of cooling of hot electrons and holes (existing as excitons) is slowed because of the presence of discrete electronic states for these electronic particles;[3] the need to conserve crystal momentum is relaxed because momentum is not a good quantum number; and[4] Auger processes (like MEG) are greatly enhanced because of increased e^-h^+ Coulomb interaction. Since electron-hole pairs created in QDs exist as excitons, the generation of multiple excitons in QDs is called multiple exciton generation (MEG) (Fig. 10). From 2001 to 2002, it was predicted[1,11] that the production of multiple e^-h^+ pairs (multiple excitons) per photon would be enhanced in QDs compared to bulk semiconductors; both a lower threshold energy ($h\upsilon_{th}$) for electron hole pair multiplication and its efficiency, η_{MEG} (defined as the number of excitons produced per additional bandgap of energy above the MEG threshold energy), would be expected to be greatly enhanced. In QDs, multiple excitons can only generate free carriers upon dissociation of the excitons, this readily occurs in various solar cell device structures.

It has been shown[22] that the threshold photon energy ($h\upsilon_{th}$) for MEG to occur and its efficiency (η_{MEG}) are related by the expression

$$h\upsilon/E_g = 1 + (1/\eta_{MEG}). \quad (12)$$

Equation (12) can be used to illustrate various MEG characteristics and to subsequently calculate the PCE for these characteristics by plotting the MEG QY vs $h\upsilon/E_g$ (Fig. 12).

Figure 12 exhibits two types of characteristics: (1) a linear function where the QY is linear with photon energy normalized to the bandgap after the threshold for MEG is reached, and (2) a staircase function (labeled M_{max}) with a threshold at $2E_g$. For the staircase function, M_{max} the QY becomes N when the photon energy $h\upsilon$ is N times E_g and remains N until the next step where it becomes N + 1 for $h\upsilon/E_g = N + 1$. The linear functions are labeled L(n) where n is the photon energy threshold in units of $h\upsilon/E_g$ and η_{MEG} = slope of the linear plot = MEG efficiency. This slope, the MEG efficiency, is the number of additional excitons produced per additional bandgap of

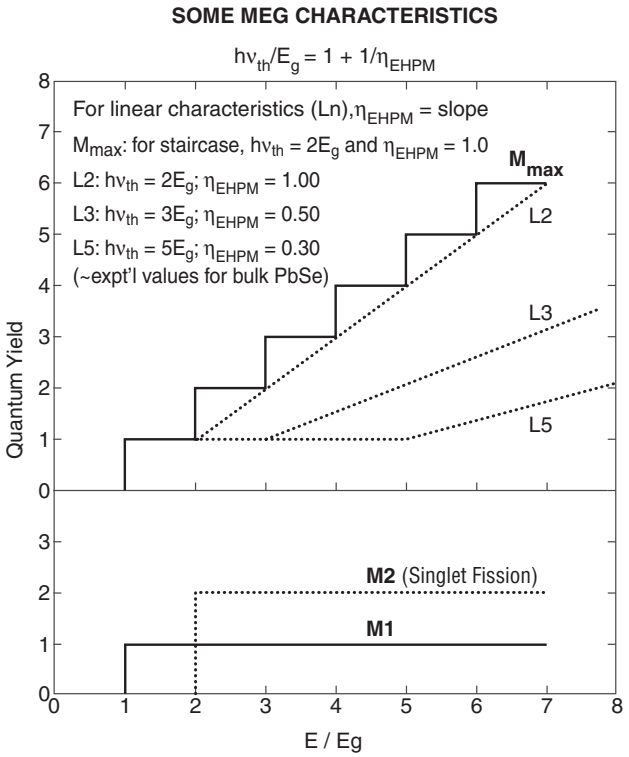

FIG. 12. MEG characteristics for quantum yield vs photon energy for different MEG threshold photon energies normalized to the bandgap ($h\upsilon_{th/Eg}$) and those for a conventional solar cell (M1). Singlet fission is discussed in Sec. IV. See text for definition of Ln and M_{max} notations. Reprinted with permission from Beard *et al.*, Nano. Lett. **10**, 3019–3027 (2010). Copyright 2010 American Chemical Society.[22]

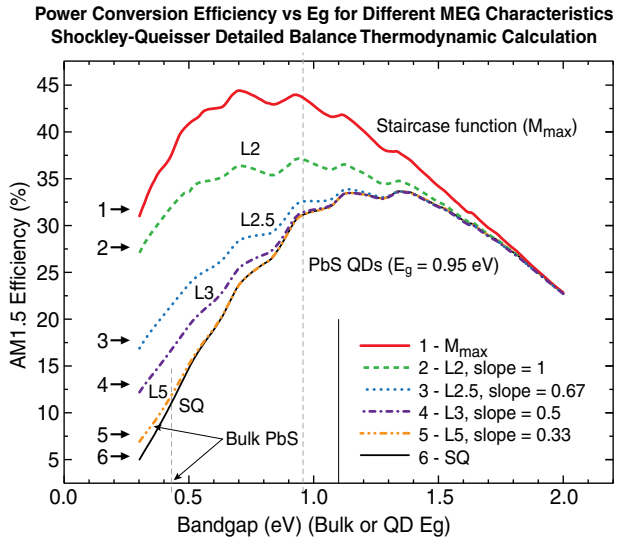

FIG. 13. S–Q PCE calculations for different MEG characteristics (Ln and M_{max}) and for conventional solar cells using bulk semiconductors without MEG. Reprinted with permission from Beard *et al.*, Nano. Lett. **10**, 3019–3027 (2010). Copyright 2010 American Chemical Society.[22]

photoexcitation energy absorbed after the MEG threshold is passed. Figure 13 presents the theoretical QY vs photon energy (normalized to the semiconductor bandgap) for values of the normalized threshold photon energy $h\upsilon_{th}/E_g = 2$, 3, and 5.

The characteristic for singlet fission (the molecular analog of MEG) is also shown and labeled as M2; M1 is the conventional characteristic of a conventional ideal solar cell with a QY = 0 below the semiconductor bandgap, jumping to a constant QW equal to 1 at and above the semiconductor bandgap value.

The S-Q type calculations for the PCE of solar cells with various MEG characteristics (nL or M_{max}) are shown in Fig. 13, along with the conventional S–Q calculation for bulk semiconductors without MEG. Figure 13 shows that for bulk semiconductors with low bandgaps (<0.5 eV, like PbS), the maximum PCE of PbS QD solar PV cells is ~3 times greater than that of PV cells made from bulk PbS. If the quantized PbS bandgap increases to 0.9 to 1.3 eV and exhibits the optimum MEG characteristic M_{max}, the maximum PCE can be ~ 4 to 5 times that of bulk PbS PV cells. Bulk semiconductors typically have photon energy thresholds ($h\upsilon_{th/Eg}$) for carrier multiplication produced by I.I. that are 3 to 5 times their bulk E_g values; therefore, they do not have the ability to greatly increase PCE through carrier multiplication.

An important result[26] in 2012 on the PCE values of QD solar cells is that theoretical S–Q type calculations show that when MEG is combined with solar concentration, the maximum PCE values increase dramatically and the peak PCE values occur with much smaller bandgaps (Fig. 14).

The results shown in Fig. 14 are for the L2 characteristic. Thus, for example, for the L2 MEG characteristic, the maximum PCE soars to 77% at a solar concentration of 1000× and a bandgap of 0.1 eV; at 500× the PCE is 74% with the same bandgap of 0.1 eV. For a more accessible bandgap of 0.6 eV at 500× the PCE is 55%. Thus, the simultaneous presence of MEG combined with solar concentration can increase the PCEs for bandgaps ranging from 0.1 to 0.6 eV

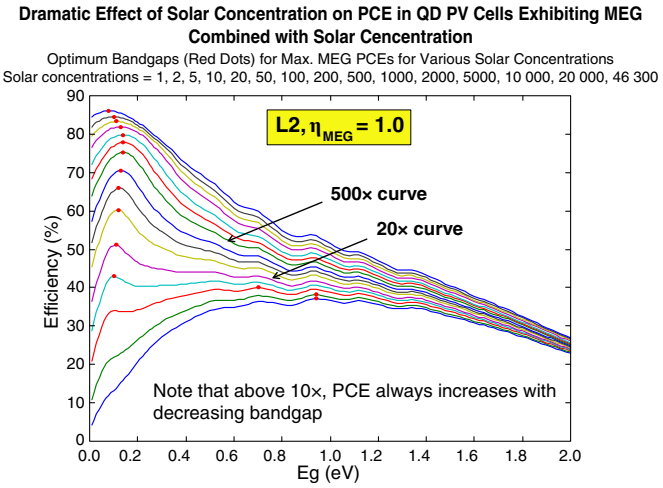

FIG. 14. Dramatic increase of PCE and dramatic red shift of optimum bandgap under solar concentration of various values ranging from 1× to 46 300× (maximum possible concentration at earth's surface). Reprinted with permission from Hanna *et al.*, J. Phys. Chem. Lett. **3**, 2857 (2012). Copyright 2012 American Chemical Society.[26]

by factors ranging from about 10× to 2×, depending upon the bulk bandgap, MEG characteristic, and the solar concentration. This is a spectacular effect, but its achievement depends upon discovering semiconductors that have the L2 or M_{max} MEG characteristic, low bandgaps (<0.75 eV), and high photostability under concentrated sunlight (50× to 1000×).

The first experimental verification of exciton multiplication in QDs was presented by Schaller and Klimov[13] in 2004 for PbSe nanocrystals (NCs). Efficient MEG has been shown to also occur in QDs of PbS, PbTe, PbSe, CdSe, InAs, Si, InP, CdTe, and CdSe/CdTe core-shell QDs.[1] The time scale for MEG has been reported to be as fast as 100 fs.[1] Ultrafast MEG, faster than the hot exciton cooling rate produced by electron–phonon interactions, can therefore beat exciton cooling and become efficient.

It is noted that in addition to many reported MEG results in semiconductor QDs, MEG has also been reported in single-wall carbon nanotubes. Theoretical considerations suggest that MEG is enhanced in nanotubes compared to QDs, in part because of stronger $e- e^-$ interactions and the absence of surface state recombination sites on the nanotube surfaces.

A critical challenge for research and development of QD-based solar cells is to understand and demonstrate QD systems that show the L2, or for even higher PCE values, the staircase MEG characteristic (M_{max}) shown in Fig. 12. In all MEG-based systems it is also critical that the rate of hot-carrier cooling be slow compared to the rates of MEG, exciton dissociation, carrier separation, transport, and extraction.

C. Photovoltaic cells based on nanowires and Qwires

An excellent review of the theoretical and experimental approaches to producing PV cells based on advanced concepts using nonequilibrium electron and phonon dynamics is presented in Ref. 48. It covers both unquantized and quantized nanowires (Qwires), as well as MEG in Qwires. The hot-carrier dynamics in 1-dimensionally confined quantum wells (QWs) is also discussed. In Ref. 49 the performance of GaAs PV cells based on 160 nm diameter wires in nanowire arrays with varying photon incidents angles was analyzed. The maximum measured PCE of this cell increased significantly with tilting due to enhanced light trapping and demonstrated significant reduced material need. Thus, at a tilt angle of 60°, the PCE was 95% of the PCE at normal incidence; with this cell illuminated at normal incidence, the PCE was 15.3%.[50] These experiments showed a reduction of a factor of 10 for the GaAs material needed for the same PCE in a conventional GaAs cell. InP nanowires topped with GaAs nanocrystals showed a PCE value of 17.8% and a short circuit current of 29.3 ma/cm^{2};[51] the latter value being very close to the best planar PV cells of the same material. An important advantage of nanowire-based solar cells is the enhanced carrier extraction along the axis of the nanowires compared to QD-based PV cells.

VI. CARRIER MULTIPLICATION VIA MEG OR SF COMBINED WITH SOLAR CONCENTRATION FOR H_2O SPLITTING FOR EXTENDED RANGES OF BANDGAPS EXHIBITING ENHANCED PCE

For photoelectrochemical (PEC) cells that can split water efficiently, two photoelectrodes need to be arranged in an optical series (tandem architecture) to provide the required photovoltage to drive the water-splitting reaction ($2H_20 = O_2 + 2H_2O$) and also achieve the highest efficiencies at any solar concentration.[16] The required photovoltage is the standard thermodynamic potential (1.23 V for water splitting) plus the overvoltage (V_0) to satisfy kinetic requirements. If both photoelectrodes generate just one electron-hole pair/photon, and the illumination intensity is one sun, the maximum thermodynamic efficiencies for H_2O splitting are 40% and 25% at overvoltages of 0 and 1.0 V, respectively. However, if the cell operates with optimum MEG (M_{max} characteristic) and the solar concentration is increased to 500×, the maximum efficiencies become 53% vs 30% for the same overvoltages of 0.0 and 1.0 V, respectively.[26] Thus, solar concentration combined with MEG greatly magnifies the beneficial effect of MEG on solar conversion efficiency producing hydrogen as a solar fuel through water splitting.[26]

A recent study[27] in 2019 explored the PCE for solar water-splitting cells with tandem PCE systems comprising MEG and/or SF layers and how solar concentration, top cell thinning, cell overvoltage (V_O), and water absorption in the incident optical path affect the PCE; the effect of photon absorption in H_2O layers is not discussed here because it is possible to design H_2O splitting cells that do not have incident photons that pass through water (Fig. 13.14 in Ref. 144 for this design configuration). MEG absorbers that produce the maximum possible PCEs, created by the ideal staircase QY characteristic (M_{max}) and a MEG threshold of $2E_g$, were examined.[27] It was shown that combining MEG or SF absorbers with solar concentration (1 to 1000 suns) and thinning the top cell to allow some photons to be absorbed in both the top and bottom layers, can achieve greatly enhanced theoretical water-splitting PCEs with values as high as 63%.

Figure 15 shows the calculated PCE contours of a tandem MEG device (with a M_{max} characteristic) under 1× solar intensity, zero overvoltage (V_O), no water path, and both with and without thinning the top cell.[27]

Under these conditions, the maximum PCE is about 47% for two tandem bandgaps of 0.5 and 1.35 eV with and without top layer thinning, respectively. Thus, the maximum PCE has the same value and the same bandgaps at 1× solar intensity for both the thinning and no thinning cases. However, high efficiencies above 40% can be achieved for bottom gaps up to 1.2 eV, Fig. 15(b), which is not true for the no thinning case [Fig. 15(a)].[27] In fact, when the top cell is thin, we observe high efficiencies in regions of Fig. 15(b), where the top cell bandgap is lower than the bottom cell bandgap (Eg2 > Eg1).[27]

With solar concentration, the broadening of bandgap ranges that yield high PCEs as a result of thinning is further and more clearly illustrated in Fig. 16,[27] where the effects of increasing solar intensity from 1 sun to 1000 suns are presented.

At the highest solar intensities between 100× to 1000×, the maximum PCEs are above 50% and the optimum bandgaps of the high PCE values at these solar intensities range over 1 eV. The finding that thinning the top cell produces exceptionally high PCEs that are extended over a very large bandgap range for both the top and bottom cell bandgaps, plus the fact that for some regimes of high PCE, the top layer bandgap is smaller than the bottom layer bandgap are very interesting and technologically important results. Thus, top cell thinning together with solar concentration greatly increases the possible range of semiconductor materials with different bandgaps that exhibit MEG to be used in high PCE H_2O splitting solar cells. Finally, it is noted that a SF–MEG tandem produces the same maximum theoretical PCE as a MEG–MEG tandem.[27]

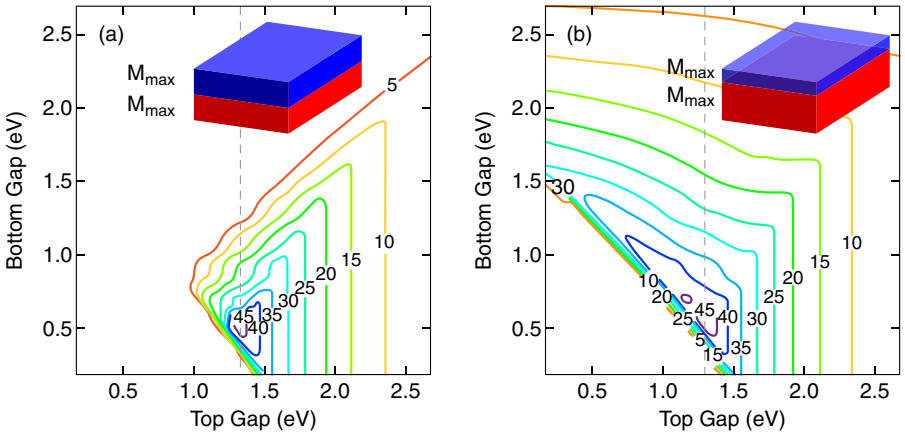

FIG. 15. PCE contours for top and bottom bandgaps for tandem MEG photocells with a maximum MEG yield. Calculations were done (a) without and (b) with thinning the top absorber at 1× solar concentration, $V_O = 0$ mV, and no water absorption. Reprinted with permission from Martinez *et al.*, J. Chem. Phys. **151**, 114111 (2019). Copyright 2019 American Institute of Publishing.[27]

For future research goals, discovering and developing new low bandgap semiconductors or SF chromophores that produce efficient carrier multiplication, improving MEG efficiencies, bringing the MEG onset close to $2E_g$, and obtaining a M_{max} staircase characteristic are major research challenges. However, the recent progress in QD design and tunability show encouraging results for MEG; an example is the CdS/PbS Janus QDs.[30] In this study, Kroupa *et al.* show that in Janus QDs, 25% of the charge carriers undergo MEG with a MEG efficiency of 98%. They also show that the onset occurs at $\sim 2E_g$, where the QY first plateaus at $1.2E_g$, then has another step-like QY increase at $3E_g$ which finally plateaus at QY = 1.4.[30]

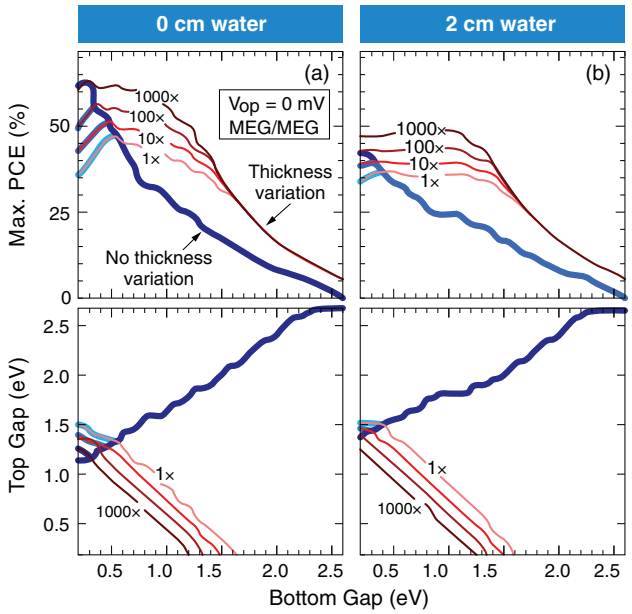

FIG. 16. Maximum PCE vs absorber bandgap plots for MEG tandem photocells as a function of AM1.5 solar concentration, thickness variation (thinning), 0 mV V_O, and with (a) 0 and (b) 2 cm water path length. The concentrations are 1 (lightest shade), 10, 100, and 1000× (darkest shade). Reprinted with permission from Martinez *et al.*, J. Chem. Phys. **151**, 114111 (2019). Copyright 2019 American Institute of Publishing.[27]

VII. BURIED JUNCTIONS AND SOLAR FUELS

Buried junctions are defined as conventional p-n, p-i-n, Schottky, nanostructured junctions, PEC junctions, or any type of photoactive junction that generates a photopotential, and which are encapsulated with inert material(s) and thus become isolated and protected from direct contact with any other material that might be detrimental to the photostability of the junction.[155] In the case of solar cells for the production of solar fuels (viz., H_2 from solar H_2O splitting as an example of the fuel), the junction is isolated from the aqueous electrolyte wherein the chemical oxidation-reduction (viz., redox) reactions occur. This feature prevents photocorrosion of the photoactive junctions for the photoanode and/or photocathode of the cell. Furthermore, the electrocatalytic surfaces where the electrochemical redox reactions occur are not those of the photoactive and charge-separating junction photomaterials but rather the photogenerated carriers are transferred to effective and photostable catalytic electrode surfaces of the protective encapsulant; this surface thus must be both a stable protective material as well as a catalyst for the desired redox reaction for fuel formation. This later feature means that in addition to

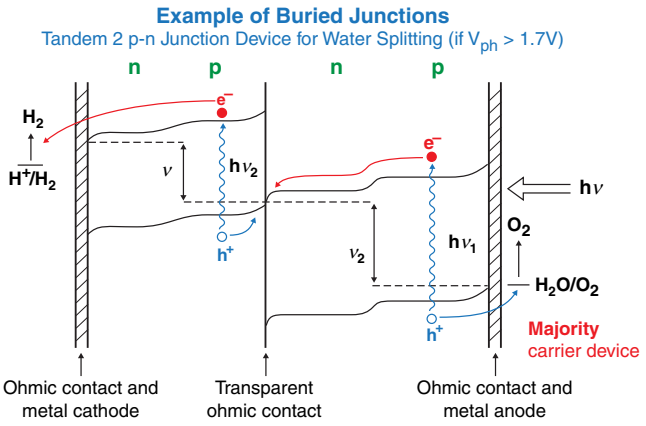

FIG. 17. Two buried tandem p-n Junctions for H_2O splitting in a Z Scheme. Reprinted from Nozik, Annu. Rev. Phys. Chem. **29**, 189 (1978). Copyright 1978 Annual Reviews, Inc.[8]

the photoprotections, the buried junction architecture ensures that the energy levels of the photogenerated electrons and holes in the photomaterial do not need to be *a priori* appropriately aligned with the redox potentials of the two oxidation and reduction half-reactions of water splitting, as is required in pure PEC systems, which operate based upon semiconductor-liquid junctions.[8,156–160] With sufficient generation of photopotential in the photomaterial to electrolyze water [1.23 V + overvoltage (Vo)], the electrochemical potentials of the catalytic surfaces protecting the photomaterial adjust automatically and instantaneously through the redistribution of charge in the Helmholtz layers at the catalytic anode and cathode surfaces that drive the water oxidation and reduction reactions, to allow appropriate charge transfer to drive the redox chemistry.[155] This removes one of the major constraints of PEC photoelectrosynthesis which requires the photomaterial to have its intrinsic redox potential (termed the flat-band potential) appropriately align the band edges of the photomaterial with the redox potential of the desired redox reaction in solution to allow efficient charge transfer and redox electrochemistry to occur.[156–160]

Another important characteristic of the buried junction approach, as described above, is that two junctions are used in a tandem configuration wherein each photomaterial in the multijunction stack has a different bandgap (or HOMO–LUMO transition) that is optimized to reduce thermalization losses of supra-band edge photogenerated carriers and maximizes conversion efficiency. The energy band diagram for two buried p-n junctions in a tandem configuration is shown as an example of a buried junction for water splitting in Fig. 17.

Figure 18 shows the energetic alignment differences between a buried junction and an unburied junction for PEC H_2O splitting. A thorough discussion of buried junctions in the context of solar fuels production is presented in Ref. 155, pages 379–385.

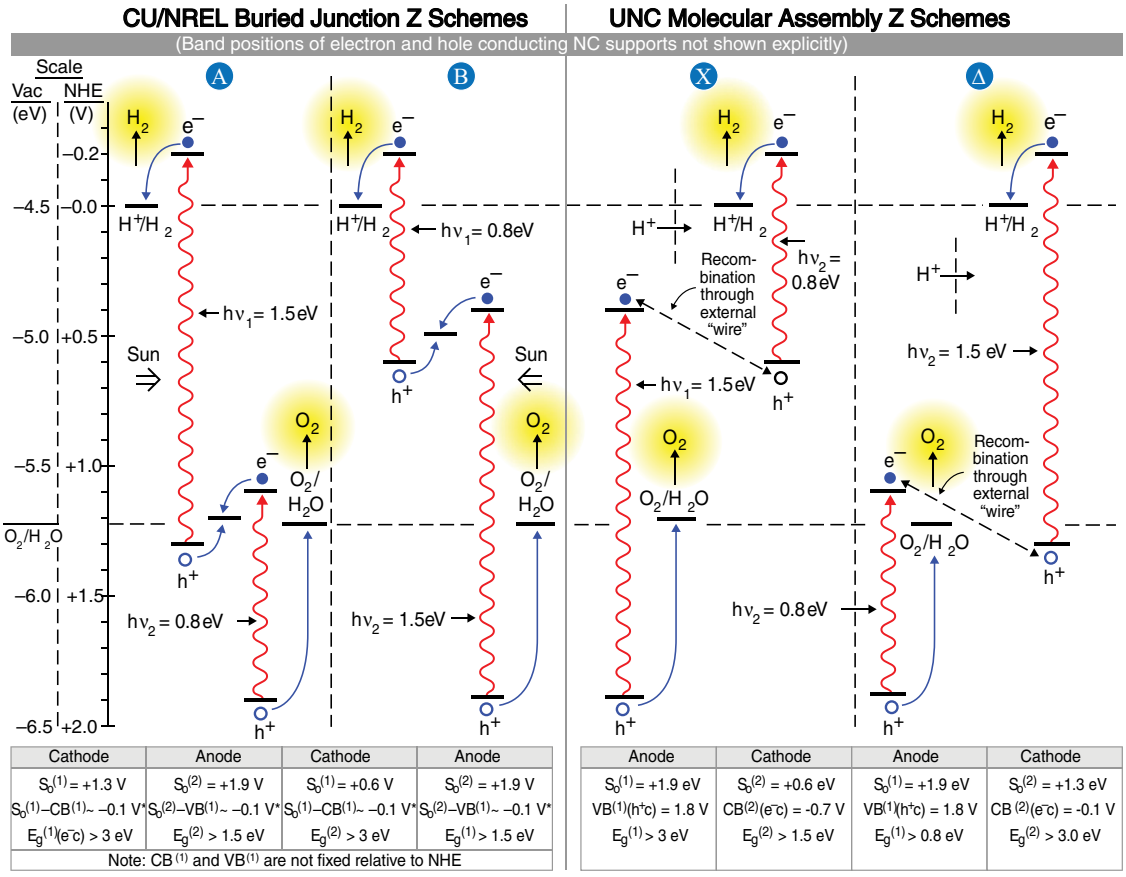

FIG. 18. Energy-level diagrams for solar H_2O splitting with two chromophores in Z schemes using buried junctions (left) and unburied PEC junctions (right). In the buried junction scheme, the two photoredox chromophores are in dye-sensitized schemes and inject their respective photogenerated electrons and holes into n- and p-type electrodes, respectively (not shown). They also provide protection of the chromophores against photodegradation, they provide catalytic surfaces for the two redox reactions, and they allow automatic alignment of the redox potentials of the injected carriers to match the required potentials to carry out the redox reactions. For the non-buried junction, the system has the usual PEC or photocatalysis energetics, where the photogenerated electrons and holes are injected directly into the redox acceptors via chromophore-molecule interactions. The catalysis must be provided by the chromophore assembly and the chromophore assembly must intrinsically provide the required fixed redox potentials for the redox reaction. The two chromophores can be supported on charge-conducting substrates with the required non-electrochemically active electron-hole recombination conducted via external electrical contacts. In both systems, one of the supporting electrodes must be transparent to light, and the energetics are different for light entering the anodic or cathodic side of the cell, as shown in the figure.

Some argue that buried junctions for solar fuel production are nothing more than a PV cell operated in electrical series with an electrochemical cell (electrolysis cell in the present example) and should be simply referred to as PV + electrolysis. Although it is true that the buried junction operates like a photovoltaic cell in that it is based on photoactive semiconductor p-n junctions, there are no external wires to carry the photogenerated current and voltage to a separate dark electrolyzer with two different electrodes for oxidation and reduction reactions. Rather, the buried junction is a photoactive monolithic structure wherein photogenerated electrons and holes are separated internally and transported to separated anodic and cathodic surfaces within the device to carry out the respective catalytic redox reactions to generate the solar fuels. It is not PV + electrolysis in the general sense of not having two spatially separate PV cells and electrolyzer cells; the cost of the latter is expected to be much higher than the buried junction architecture.

VIII. SOLAR CELL PHOTOELECTRODES COMPOSED OF QUANTUM DOT ARRAYS

In the QD array configuration, the QDs are formed into an ordered 3D array with inter-QD spacing sufficiently small that strong electronic coupling occurs and 3D minibands may form to allow long-range carrier transport.[12,23] The system is a 3D analog to the 1D superlattice, and miniband structures discussed above in "Energy Levels and Density of States in Quantum Wells and Superlattices." The delocalized quantized 3D miniband electronic states could be expected to slow the carrier cooling and also permit the transport and collection of hot carriers to produce a higher photopotential in a photovoltaic cell or in a photoelectrochemical cell in which the 3D QD array is the photoelectrode.[12,23] Also, MEG is expected to occur in the QD arrays, enhancing the photocurrent.[12] The PCEs of such MEG- or SF-based arrays for both PV cells and cells for solar fuels are expected to be significantly enhanced and generally of lower cost.

Significant progress has been made in forming 3D arrays of both colloidal and Stranski-Krastanov (SK) II-VI and III-V QDs.[23] The former has been formed via evaporation and crystallization of colloidal QD solutions containing a near-uniform QD size distribution. The crystallization of QD solids from broader size distributions leads to close-packed QD solids, but with a high degree of disorder. To improve disorder, arrays of SK QDs have been formed by successive epitaxial deposition of SK QD layers; after the first layer of SK QDs is formed, successive layers tend to form with the QDs in each layer aligned on top of each other. Studies of the properties of QD arrays are under study. Major theoretical and experimental issues under study are the nature of the electronic states as a function of interdot distance, array order vs disordered arrays, QD shape, surface states, surface structure/passivation, surface chemistry, and transport properties of QD arrays.

IX. CONCLUSIONS

The progress in the development and global installation of solar PV modules, based primarily on Si cells, has been dramatic; in 1978, the levelized cost of PV electrical energy was about \$8/kWh, while in 2020, it was less than \$0.05/kWh (utility scale). This is due to great reductions in PV module production costs (due to the economy of scale) and increases in module power conversion efficiency. In 2019, solar PV power had the highest new installation volume of any other electrical power source in the U.S., including coal, nuclear, and hydro. But the progress in producing solar fuels through splitting H_2O into H_2 and O_2 or via artificial photosynthesis, whereby H_2O reacts with CO_2 to produce carbon-based liquid and gaseous fuels, has not progressed to a commercial/industrial scale since 1975 (unlike the PV industry). Laboratory scale R&D on various aspects of artificial photosynthesis has indeed progressed, but no solar fuels industry yet exists after >45 years of R&D. Since power conversion efficiency of the solar irradiance into the free energy of chemical bonds in fuels or in electricity is a major factor in the cost of solar photon conversion, it is essential to make this efficiency as high as possible, and well above the Shockley–Queisser thermodynamic limit. This is true for PV electricity in order for it to meet the future U.S. Department of Energy (DOE) goal of \$0.03/kWh, as well as for liquid and gaseous solar fuels to be competitive with fossil-based and bio-based fuels. Several approaches toward exceeding the S–Q PCE limit for both PV and solar fuels production are feasible and under investigation today. These include hot-carrier solar cells, utilizing quantization effects in semiconductor nanostructures, photogenerated charge-carrier multiplication through multiple exciton generation (MEG) from single photons in semiconductor-based quantum dot solar cells or singlet fission (SF) in molecular chromophores, MEG and/or SF combined with solar concentration and control of photomaterial thickness in double junction cells for solar fuels, and buried junctions.

ACKNOWLEDGMENTS

The author gratefully acknowledges support for this work through the solar photochemistry program within the Division of Chemical Sciences, Geosciences, and Biosciences, Office of Basic Energy Sciences, Office of Science within the United States Department of Energy through Contract No. DE-AC36-08G028308. The views expressed in the article do not necessarily represent the views of the DOE or the United States Government. The United States Government retains and the publisher, by accepting the article for publication, acknowledges that the United States Government retains a nonexclusive, paid-up, irrevocable, worldwide license to publish or reproduce the published form of this work, or allow others to do so, for United States Government purposes.

The author also gratefully acknowledges colleagues at the National Renewable Energy Laboratory (NREL) and elsewhere for collaboration and discussions on all subjects covered by this review and associated research by the author with these collaborators: Matt Beard, Joey Luther, Randy Ellingson, Alexander Efros, Andrew Shabaev, Mark Hanna, Yossi Rosenwaks, Justin Johnson, Olga Micic (deceased), Jeff Blackburn, Richard Ahrenkiel, Victor Klimov, Ferd Williams (deceased), Daryl Boudreaux, John Turner, Jerry Cooper, Bruce Parkinson, Chung Tang, Robert Ross, Matt Law, Garry Rumbles, Sue Ferrer, Tim Lian and many former graduate students (especially Tijana Rajh, Jeff Blackburn, Jim Murphy, Pingrong Yu, Octavi Semonin, Dan Krupa, Barbara Hughes, Aaron Midgett, Ashley Marshall, Helen Chappell, Joe Ryerson, and Marissa Martinez), as well as many other former postdoctoral associates at the University of Colorado and NREL (Barton Smith, David Szymd, Ehud Poles, Julian Sprague, Andreas Meier Jianbo Gao, Candy Mercado, D. M. Sagar, Kate Gerth, Kelly Knutsen, Don Selmarten, Arie Zaban, Mark Peterson, and Qing Song).

DATA AVAILABILITY

Data sharing is not applicable to this article as no new data were created or analyzed in this study.

REFERENCES

[1]A. J. Nozik, "Spectroscopy and hot electron relaxation dynamics in semiconductor quantum dots," Ann. Rev. Phys. Chem. **52**, 193–231 (2001).
[2]J. I. Pankove, *Optical Processes in Semiconductors* (Dover, New York, 1975).
[3]S. Sze, *Physics of Semiconductor Devices* (Wiley, New York, 1981).
[4]W. Shockley and H. J. Queisser, "Detailed balance limit of efficiency of p-n junction solar cells," J. Appl. Phys. **32**, 510 (1961).
[5]M. A. Green, *Solar Cells: Operating Principles, Technology and System Applications* (Prentice-Hall, Englewood Cliffs, 1992).
[6]J. Nelson, *The Physics of Solar Cells* (Imperial College Press, London, 2003).
[7]P. Wurfel, *Physics of Solar Cells: From Basic Principles to Advanced Concepts* (WILEY-VCH, Weinheim, 2010).
[8]A. J. Nozik, "Photoelectrochemistry: applications to solar energy conversion," Annu. Rev. Phys. Chem. **29**, 189–222 (1978).
[9]F. Williams and A. J. Nozik, "Irreversibilities in the mechanism of photoelectrolysis," Nature **271**, 137–139 (1978).
[10]R. T. Ross and A. J. Nozik, "Efficiency of hot-carrier solar energy converters," J. Appl. Phys. **53**, 3813 (1982).
[11]D. S. Boudreaux, F. Williams, and A. J. Nozik, "Hot carrier injection at semiconductor-electrolyte junctions," J. Appl. Phys. **51**, 2158 (1980).
[12]A. J. Nozik, "Quantum dot solar cells," Physica E **14**, 115–120 (2002).
[13]R. Schaller and V. L. Klimov, "High efficiency carrier multiplication in PbSe nanocrystals: Implications for solar energy conversion," Phys. Rev. Lett. **92**, 186601 (2004).
[14]R. J. Ellingson, M. C. Beard, J. Johnson, P. Yu, O. I. Mićić, A. J. Nozik, A. J. Shabaev, and A. L. Efros, "Highly efficient multiple exciton generation in colloidal PbSe and PbS quantum dots," Nano Lett. **5**, 865–871 (2005).
[15]A. J. Nozik, "Exciton multiplication and relaxation dynamics in quantum dots: Applications to ultrahigh-efficiency solar photon conversion," Inorg. Chem. **44**, 6893–6899 (2005).
[16]M. C. Hanna and A. J. Nozik, "Solar conversion efficiency of photovoltaic and photoelectrolysis cells with carrier multiplication absorbers," J. Appl. Phys. **100**, 074510 (2006).
[17]A. Shabaev, AI. L. Efros, and A. J. Nozik, "Multi-exciton generation by a single photon in nanocrystals," Nano Lett. **6**, 2856–2863 (2006).
[18]A. J. Nozik, "Multiple exciton generation in semiconductor quantum dots," Chem. Phys. Lett. **457**, 3–11 (2008).
[19]M. C. Beard, A. H. Ip, J. M. Luther, E. H. Sargent, and A. J. Nozik, "Quantum confined semiconductors for enhancing solar photoconversion through multiple Exciton Generation," in *Advanced Concepts in Photovoltaics* (Royal Society of Chemistry, Cambridge, 2014), Chap. 11.
[20]M. C. Beard, K. K. Knutsen, P. Yu, J. Luther, Q. Song, R. J. Ellingson, and Nozik, A. J., "Multiple exciton generation in colloidal silicon nanocrystals," Nano Lett. **7**, 2506–2512 (2007).
[21]A. J. Nozik, "Nanoscience and nanostructures for photovoltaics and solar fuels," Nano Lett. **10**, 2735–2741 (2010).
[22]M. C. Beard, A. G. Midgett, M. C. Hanna, J. M., Luther, B. K. Hughes, and A. J. Nozik, "Comparing multiple exciton generation in quantum dots to impact ionization in bulk semiconductors: Implications for enhancement of solar energy conversion," Nano Lett. **10**, 3019–3027 (2010).
[23]A. J. Nozik, M. C. Beard, J. M. Luther, M. Law, R. J. Ellingson, and J. C. Johnson, "Semiconductor quantum dots and quantum dot arrays and applications of multiple exciton generation to third-generation photovoltaic solar cells," Chem. Rev. **110**, 6873–6890 (2010).
[24]O. E. Semonin, J. M. Luther, S. Choi, H.-Y. Chem, J. Gao, A. J. Nozik, and M. C. Beard, "Peak external photocurrent quantum efficiency exceeding 100% via MEG in a quantum dot solar cell," Science **334**, 1530–1533 (2011).
[25]J. T. Stewart, L. Padilha, L. A. Qazilbash, M. Mumtaz, J. M. Pietryga, A. G. Midgett, L. M. Luther, M. C. Beard, A. J. Nozik, and V. I. Klimov, "Comparison of carrier multiplication yields in PbS and PbSe Nanocrystals: The role of competing energy loss processes," Nano Lett. **12**, 622–628 (2012).
[26]M. C. Hanna, M. C. Beard, and A. J. Nozik, "Effect of solar concentration on the thermodynamic power conversion efficiency of quantum-dot solar cells exhibiting multiple exciton generation," J. Phys. Chem. Lett **3**, 2857–2862 (2012).
[27]M. Martinez, A. J. Nozik, and M. C. Beard, "Theoretical limits of multiple excitation generation and singlet fission tandem devices for solar water splitting," J. Chem. Phys. **151**, 114111 (2019).
[28]M. C. Beard, J. M. Luther, O. Semonin, and A. J. Nozik, "Third generation photovoltaics based on multiple exciton generation in quantum confined semiconductors," Acc. Chem. Res. **46**, 1252–1260 (2013).
[29]M. C. Beard, J. M. Luther, and A. J. Nozik, "The promise and challenge of nanostructured solar cells," Nat. Nanotech **9**, 951–954 (2014).
[30]D. M. Kroupa, G. F. Pach, M. Vörös, F. Giberti, B. D. Chernomordik, R. W. Crisp, A. J. Nozik, J. C. Johnson, R. Singh, V. I. Klimov, G. Galli, and M. C. Beard, "Enhanced multiple exciton generation in PbS|CdS Janus-like heterostructured nanocrystals," ACS Nano **12**, 10084–10094 (2018).
[31]Y. Yan, R. Crisp, J. Gu, B. D. Chernomordik, G. F. Pach, A. R. Marshall, J. A. Turner, and M. C. Beard, "Multiple exciton generation for photoelectrochemical hydrogen evolution reactions with quantum yields exceeding 100%," Nat. Energy **2**, 17052 (2017).
[32]W. S. Pelouch, R. J. Ellingson, P. E. Powers, C. L. Tang, D. M. Szmyd, and A. J. Nozik, "Comparison of hot-carrier relaxation in quantum wells and bulk GaAs at high carrier densities," Phys. Rev. B **45**, 1450 (1992).
[33]Y. Rosenwaks, M. C. Hanna, D. H. Levi, D. M. Szmyd, R. K. Ahrenkiel, and A. J. Nozik, "Hot carrier cooling in GaAs: Quantum wells versus bulk," Am. J. Phys. Rev. B **48**, 14675 (1993).
[34]M. C. Hanna, L. Zhengao, and A. J. Nozik, "Hot Carrier Solar Cells," AIP Conf. Proc. **404**, 309 (1997).
[35]I. Paci, J. C. Johnson, X. Chen, G. Rana, D. Popović, D. E. David, A. J. Nozik, M. A. Ratner, and J. J. Michl, "Singlet fission for dye-sensitized solar cells: Can a suitable sensitizer be found," J. Am. Chem. Soc. **128**, 16546–16553 (2006).
[36]M. B. Smith and J. Michl, "Singlet fission," Chem. Rev. **110**, 6891–6936 (2010).
[37]J. C. Johnson, A. J. Nozik, and J. Michl, "High triplet yield high triplet yield from singlet fission in a thin film of 1,3-Diphenylisobenzofuran," J. Am. Chem. Soc. **132**, 16302–16303 (2010).
[38]C. Wang and J. Tauber, "High-yield singlet fission in a zeaxanthin aggregate observed by picosecond resonance raman spectroscopy," J. Am. Chem. Soc. **132**, 13988–13991 (2010).
[39]M. B. Smith and J. Michl, "Recent advances in singlet fission," Annu. Rev. Phys. Chem. **64**, 361–386 (2013).
[40]J. C. Johnson and J. Michl, "1,3 Diphenylisobenzofuran: A model chromophore for singlet fission," Top. Curr. Chem. **375**, 80 (2017).
[41]R. Dingle, *Semiconductors and Semimetals* (Academic Press, New York, 1987), Vol. 24.
[42]R. Dingle, A. C. Gossard, and W. Wiegmann, "Direct observation of superlattice formation in a semiconductor heterostructure," Phys. Rev. Lett. **34**, 1327 (1975).
[43]R. Dingle, W. Wiegmann, and C. H. Henry, "Quantum states of confined carriers in very thin $Al_xGa_{1-x}As$-GaAs-$Al_xGa_{1-x}As$ heterostructures," Phys. Rev. Lett. **33**, 827 (1974).
[44]E. L. Lifshitz, M. Bashouti, V. Kloper, A. Kigel, M. S. Eisen, and S. Berger, "Synthesis and characterization of PbSe quantum wires, multipods, quantum rods, and cubes," Nano Lett **3**, 857–862 (2003).
[45]D. Tedeschi, M. De Luca, H. A. Fonseka, Q. Gao, F. Mura, H. H. Tan, S. Rubini, F. Martelli, C. Jagadish, M. Capizzi, and A. Polimeni, "Long-lived hot carriers in III-V nanowires," Nano Lett. **16**, 3085–3093 (2016).
[46]C. K. Yong, J. Wong-Leung, H. J. Joyce, J. Lloyd-Hughes, Q. Gao, H. H. Tan, C. Jagadish, M. B. Johnston, and L. M. Herz, "Direct observation of charge-carrier heating at WZ-ZB InP nanowire heterojunctions," Nano Lett. **13**, 4280–4287 (2013).
[47]I. A. Shojaei, S. Linser, G. Jnawali, N. Wickramasuriya, H. E. Jackson, L. M. Smith, F. Kargar, A. A. Balandin, X. Yuan, P. Caroff, H. H. Tan, and C. Jagadish, "Strong hot carrier effects in single nanowire heterostructures," Nano Lett. **19**, 5062–5069 (2019).
[48]R. Hathwar, Y. Zou, C. Jirauschek, and S. M. Goodnick, "Nonequilibrium electron and phonon dynamics in advanced concept solar cells," J. Phys. D: Appl. Phys. **52**, 093001 (2019).
[49]O. M. Ghahfarokhi, N. Anttu, L. Samuelson, and I. Aberg, "Performance of GaAs nanowire array solar cells for varying incidence angles", IEEE J. Photovolt. **6**, 1502–1508 (2016).

[50]Åberg, G. Vescovi, D. Asoli, U. Naseem, J. P. Gilboy, C. Sundvall, A. Dahlgren, K. E. Svensson, N. Anttu, M. T. Björk, and L. Samuelson "A GaAs nanowire array solar cell with 15.3% efficiency with 1 sun", IEEE J. Photovolt. **6**, 185–190 (2016).
[51]D. van Dam, N. J. J. van Hoof, Y. Cui, P. J. van Veldhoven, E. P. A M. Bakkers, J. G. Rivas, and J. E M. Haverkort, "High-efficiency nanowire solar cells with omnidirectionally enhanced absorption due to self-aligned indium-Tin-oxide Mie scatterers" ACS Nano **10**, 11414–11419 (2016).
[52]P. D. Cunningham, J. E. Boercker, E. E. Foos, M. P. Lumb, A. R. Smith, J. G. Tischler, and J. S. Melinger, "Correction to enhanced multiple exciton generation in quasi-one-dimensional semiconductors" Nano Lett. **13**, 3003 (2013).
[53]P. D. Cunningham, J. E. Boercker, E. E. Foos, M. P. Lumb, A. R. Smith, J. G. Tischler, and J. S. Melinger, "Enhanced multiple exciton generation in quasi-one-dimensional semiconductors" Nano Lett. **11** 3476–3481 (2011).
[54]R. D. J. Miller, G. McLendon, A. J. Nozik, W. Schmickler, and F. Willig, *Surface Electron Transfer Processors* (VCH Publishers, New York, 1995).
[55]G. Bastard, "Superlattice band structure in the envelope-function approximation," Phys. Rev. B. **24**, 5693 (1981).
[56]G. Bastard, "Theoretical investigations of superlattice band structure in the envelope-function approximation," Phys. Rev. B. **25**, 7584 (1982).
[57]G. Bastard, *Wave Mechanics Applied to Semiconductor Heterostructures* (Halsted Press, New York, 1988).
[58]C. Weisbuch and B. Vinter, *Quantum Semiconductor Structures* (Academic Press, New York, 1991).
[59]L. E. Brus, "Electron-electron and electron-hole interactions in small semiconductor crystallites: The size dependence of the lowest excited electronic state," J. Chem. Phys. **80**, 4403 (1984).
[60]L. E. Brus, "Electronic wave functions in semiconductor clusters: Experiment and theory," J. Phys. Chem. **90**, 2555–2560 (1986).
[61]O. I. Mićić, H. M. Cheong, H. Fu, A. Zunger, J. R. Sprague, A. Mascarenhas, and A. J. Nozik, "Size-dependent spectroscopy of InP quantum Dots," J. Phys. Chem. B **101**, 4904–4912 (1997).
[62]D. C. Edelstein, C. L. Tang, and A. J. Nozik, "Picosecond relaxation of hot-carrier distributions in GaAs/GaAsP strained-layer superlattices," Appl. Phys. Lett. **51**, 48 (1987).
[63]M. J. Rosker, F. W. Wise, and C. L. Tang, "Femtosecond optical measurement of hot-carrier relaxation in GaAs, AlGaAs, and GaAs/AlGaAs multiple quantum well structures," Appl. Phys. Lett. **49**, 1726 (1986).
[64]Z. Y. Xu and C. L. Tang, "Picosecond relaxation of hot carriers in highly photoexcited bulk GaAs and GaAs-AlGaAs multiple quantum wells," Appl. Phys. Lett. **44**, 692 (1984).
[65]J. Christen and D. Bimberg, "Line shapes of intersubband and excitonic recombination in quantum wells: Influence of final-state interaction, statistical broadening, and momentum conservation," Phys. Rev. B **42**, 7213 (1990).
[66]W. Cai, M. C. Marchetti, and M. Lax, "Nonequilibrium electron-phonon scattering in semiconductor heterojunctions," Phys. Rev. B **34**, 8573 (1986).
[67]J. F. Ryan, R. A. Taylor, A. J. Turberfield, A. Maciel, J. M. Worlock, A. C. Gossard, and W. Wiegmann, "Time-resolved photoluminescence of two-dimensional hot carriers in GaAs-AlGaAs heterostructures," Phys. Rev. Lett. **53**, 1841 (1984).
[68]A. J. Nozik, C. A. Parsons, D. J. Dunlavy, B. M. Keyes, and R. K. Ahrenkiel, "Dependence of hot electron luminescence on barrier thickness in GaAs/AlGaAs superlattices and multiple quantum wells," Solid State Commun. **75**, 297–301 (1990).
[69]V. B. Campos, S. Das Sarma, and M. A. Stroscio, "Phonon-confinement effect on electron energy loss in one-dimensional quantum wires," Phys. Rev. B **46**, 3849 (1992).
[70]R. P. Joshi and D. K. Ferry, "Hot-phonon effects and interband relaxation processes in photoexcited GaAs quantum wells," Phys. Rev. B **39**, 1180 (1989).
[71]P. Lugli and S. M. Goodnick, "Nonequilibrium longitudinal-optical phonon effects in GaAs-AlGaAs quantum wells," Phys. Rev. Lett. **59**, 716 (1987).
[72]G. Conibeer, J.-F. Guillemoles, F. Yu, and H. Levard, in *Advanced Concepts in Photovoltaics* (Royal Society of Chemistry, Cambridge, 2014), Chap. 12.
[73]G. Conibeer, R. Patterson, L. Huang, J.-F. Guillemoles, D. Kőnig, S. Shrestha, and M. A. Green, "Modelling of hot carrier solar cell absorbers," Sol. Energy Mater. Sol. Cells **94**, 1516–1521 (2010).
[74]H. Esmaielpour, K. R. Dorman, D. K. Ferry, T. D. Mishima, M. B. Santos, V. R. Whiteside, and I. R. Sellers, "Exploiting intervalley scattering to harness hot carriers in III-V solar cells," Nat. Energy **5**, 336–343 (2020).
[75]D. K. Ferry, "In search of a true hot carrier solar cell," Semicond. Sci. Tech. **34**, 44001 (2019).
[76]I. Sellers, "Special Issue on 'Recent progress towards the realization of hot carrier solar cells,'" Semicond. Sci. Tech. **34–35** (2019–2020).
[77]D. K. Ferry, S. M. Goodnick, V. R. Whiteside, and I. R. Sellers, "Challenges, myths, and opportunities in hot carrier solar cells," J. Appl. Phys. **128**, 220903 (2020).
[78]U. Bockelmann and G. Bastard, "Phonon scattering and energy relaxation in two-, one-, and zero-dimensional electron gases," Phys. Rev. B **42**, 8947 (1990).
[79]U. Bockelmann and T. Egeler, "Electron relaxation in quantum dots by means of Auger processes," Phys. Rev. B **46**, 15574 (1992).
[80]H. Benisty, "Reduced electron-phonon relaxation rates in quantum-box systems: Theoretical analysis," Phys. Rev. B **51**, 13281 (1995).
[81]H. Benisty, C. M. Sotomayor-Torrès, and C. Weisbuch, "Intrinsic mechanism for the poor luminescence properties of quantum-box systems," Phys. Rev. B **44**, 10945 (1991).
[82]AI. L. Efros, V. A. Kharchenko, and M. Rosen, "Breaking the phonon bottleneck in nanometer quantum dots: Role of Auger-like processes," Solid State Commun. **93**, 281–284 (1995).
[83]I. Vurgaftman and J. Singh, "Effect of spectral broadening and electron-hole scattering on carrier relaxation in GaAs quantum dots," Appl. Phys. Lett. **64**, 232 (1994).
[84]P. C. Sercel, "Multiphonon-assisted tunneling through deep levels: A rapid energy-relaxation mechanism in nonideal quantum-dot heterostructures," Phys. Rev. B. **51**, 14532 (1995).
[85]T. Inoshita and H. Sakaki, "Electron relaxation in a quantum dot: Significance of multiphonon processes," Phys. Rev. B **46**, 7260 (1992).
[86]T. Inoshita and H. Sakaki, "Density of states and phonon-induced relaxation of electrons in semiconductor quantum dots," Phys. Rev. B **56**, R4355 (1997).
[87]K. Mukai and M. Sugawara, *Self-Assembled InGaAs/GaAs Quantum Dots* (Academic Press, San Diego, 1999), Vol. 20.
[88]P. Guyot-Sionnest, M. Shim, C. Matranga, and M. Hines, "Intraband relaxation in CdSe quantum dots," Phys. Rev. B **60**, R2181 (1999).
[89]P. D. Wang, C. M. Sotomayor-Torres, H. McLelland, S. Thoms, M. Holland, and C. R. Stanley, "Photoluminescence intensity and multiple phonon Raman scattering in quantum dots: Evidence of the bottleneck effect," Surf. Sci. **305**, 585–590 (1994).
[90]K. Mukai and M. Sugawara, "Slow carrier relaxation among sublevels in annealed self-formed InGaAs/GaAs quantum dots," Jpn. J. Appl. Phys. **37**, 5451 (1998).
[91]K. Mukai, N. Ohtsuka, H. Shoji, and M. Sugawara, "Emission from discrete levels in self-formed InGaAs/GaAs quantum dots by electric carrier injection: Influence of phonon bottleneck," Appl. Phys. Lett. **68**, 3013 (1996).
[92]R. Heitz, M. Veit, N. N. Ledentsov, A. Hoffmann, D. Bimberg, V. M. Ustinov, P. S. Kop'ev, and Zh. I. Alferov, "Energy relaxation by multiphonon processes in InAs/GaAs quantum dots," Phys. Rev. B **56**, 10435 (1997).
[93]B. N. Murdin, A. R. Hollingworth, M. Kamal-Saadi, R. T. Kotitschke, C. M. Ciesla, C. R. Pidgeon, P. C. Findlay, H. P. M. Pellemans, C. J. G. M. Langerak, A. C. Rowe, R. A. Stradling, and E. Gornik, "Suppression of LO phonon scattering in Landau quantized quantum dots," Phys. Rev. B **59**, R7817 (1999).
[94]R. Heitz, A. Kalburge, Q. Xie, M. Grundmann, P. Chen, A. Hoffmann, A. Madhukar, and D. Bimberg, "Excited states and energy relaxation in stacked InAs/GaAs quantum dots," Phys. Rev. B **57**, 9050 (1998).
[95]K. Mukai, N. Ohtsuka, H. Shoji, and M. Sugawara, "Phonon bottleneck in self-formed InxGa1−xAs/GaAs quantum dots by electroluminescence and time-resolved photoluminescence," Phys. Rev. B **54**, R5243 (1996).
[96]H. Yu, S. Lycett, C. Roberts, and R. Murray, "Time resolved study of self-assembled InAs quantum dots," Appl. Phys. Lett. **69**, 4087 (1996).
[97]M. Sugawara, K. Mukai, and H. Shoji, "Effect of phonon bottleneck on quantum-dot laser performance," Appl. Phys. Lett. **71**, 2791 (1997).
[98]F. Adler, M. Geiger, A. Bauknecht, F. Scholz, H. Schweizer, and M. H. Pilkuhn, "Optical transitions and carrier relaxation in self assembled InAs/GaAs quantum dots," J. Appl. Phys. **80**, 4019 (1996).

[99]F. Adler, M. Geiger, A. Bauknecht, D. Haase, P. Ernst, A. Dörnen, F. Scholz, and H. Schweizer, "Self-assembled InAs/GaAs quantum dots under resonant excitation," J. Appl. Phys. **83**, 1631 (1998).
[100]K. Brunner, U. Bockelmann, G. Abstreiter, M. Walther, G. Böhm, G. Tränkle, and G. Weimann, "Photoluminescence from a single GaAs/AlGaAs quantum dot," Phys. Rev. Lett. **69**, 3216 (1992).
[101]K. Kamath, H. Jiang, D. Klotzkin, J. Phillips, T. Sosnowski, T. Norris, J. Singh, and P. Bhattacharya, "Strain tensor, electronic spectra and carrier dynamics in In(Ga)As/GaAs self-assembled quantum dots," Inst. Phys. Conf. Ser. (Compound Semicond. Symp. 1997). **156**, 525 (1998).
[102]T. H. Gfroerer, M. D. Sturge, K. Kash, J. A. Yater, A. S. Plaut, P. S. Lin, L. T. Florez, J. P. Harbison, S. R. Das, and L. Lebrun, "Slow relaxation of excited states in strain-induced quantum dots," Phys. Rev. B **53**, 16474 (1996).
[103]J. Bellessa, V. Voliotis, R. Grousson, D. Roditchev, C. Gourdon et al., Proc. Int. Conf. Phys. Semicond. Singapore: World Sci. **178**, 763 (1998).
[104]I. Gontijo, G. S. Buller, J. S. Massa, A. C. Walker, S. V. Zaitsev, N. Yu. Gordeev, V. M. Ustinov, and P. S. Kop'ev, "Time-resolved photoluminescence and carrier dynamics in vertically-coupled self-assembled quantum dots," Jpn. J. Appl. Phys. **38**, 674 (1999).
[105]X.-Q. Li, H. Nakayama, and Y. Arakawa, "Lifetime of confined LO phonons in quantum dots and its impact on phonon bottleneck issue," Jpn. J. Appl. Phys. **38**, 473 (1999).
[106]K. Kral and Z. Khas, "Electron self-energy in quantum dots," Physica Status Solidi B **208**, R5 (1998).
[107]M. Lowisch, M. Rabe, F. Kreller, and F. Henneberger, "Electronic excitations and longitudinal optical phonon modes of self-assembled CdSe quantum dots revealed by microprobe studies," Appl. Phys. Lett. **74**, 2489 (1999).
[108]V. I. Klimov and D. W. McBranch, "Femtosecond 1p-to-1s electron relaxation in strongly confined semiconductor nanocrystals," Phys. Rev. Lett. **80**, 4028 (1998).
[109]D. Bimberg, N. N. Ledentsov, M. Grundmann, R. Heitz, J. Boehrer, V. M. Ustinov, P. S. Kop'ev, and Zh. I. Alferov, "Luminescence properties of semiconductor quantum dots," J. Lumin. **72**, 34–37 (1997).
[110]B. Ohnesorge, M. Albrecht, J. Oshinowo, A. Forchel, and Y. Arakawa, "Rapid carrier relaxation in self-assembled $In_xGa_{1-x}As$/GaAs quantum dots," Phys. Rev. B **54**, 11532 (1996).
[111]J. H. H. Sandmann, S. Grosse, G. von Plessen, J. Feldmann, G. Hayes, R. Phillips, H. Lipsanen, M. Sopanen, and J. Ahopelto, "Ultrafast relaxation dynamics in strain-induced quantum dots," Physica Status Solidi B **204**, 251–254 (1997).
[112]R. Heitz, M. Veit, A. Kalburge, Q. Zie, M. Grundmann, P. Chen, N. N. Ledentsov, A. Hoffmann, A. Madhukar, D. Bimberg, V. M. Ustinov, P. S. Kop'ev, and Zh. I. Alferov, "Hot carrier relaxation in InAs/GaAs quantum dots," Physica E **2**, 578–582 (1998).
[113]X.-Q. Li and Y. Arakawa, "Anharmonic decay of confined optical phonons in quantum dots," Phys. Rev. B **57**, 12285 (1998).
[114]T. S. Sosnowski, T. B. Norris, H. Jiang, J. Singh, K. Kamath, and P. Bhattacharya, "Rapid carrier relaxation in In0.4Ga0.6As/GaAs quantum dots characterized by differential transmission spectroscopy," Phys. Rev. B **57**, R9423 (1998).
[115]U. Woggon, H. Giessen, F. Gindele, O. Wind, B. Fluegel, and N. Peyghambarian, "Ultrafast energy relaxation in quantum dots," Phys. Rev. B **54**, 17681 (1996).
[116]A. Meier, D. C. Selmarten, K. Siemoneit, B. B. Smith, and A. J. Nozik, "Fast electron transfer across semiconductor−molecule interfaces: GaAs/Co(Cp)2+/0," J. Phys. Chem. B **103**, 2122–2141 (1999).
[117]A. Meier, S. S. Kocha, M. C. Hanna, A. J. Nozik, K. Siemoneit, R. Reineke-Koch, and R. Memming, "Electron transfer rate constants for majority electrons at GaAs and GaInP2 semiconductor−liquid interfaces," J. Phys. Chem. B **101**, 7038–7042 (1997).
[118]S. J. Diol, E. Poles, Y. Rosenwaks, and R. J. D. Miller, "Electron-transfer dynamics at GaAs surface quantum wells," J. Phys. Chem. B **102**, 6193–6201 (1998).
[119]V. I. Klimov, D. W. McBranch, C. A. Leatherdale, and M. G. Bawendi, "Electron and hole relaxation pathways in semiconductor quantum dots," Phys. Rev. B **60**, 13740 (1999).
[120]V. I. Klimov, "Optical nonlinearities and ultrafast carrier dynamics in semiconductor nanocrystals," J. Phys. Chem. B **104**, 6112–6123 (2000).
[121]V. I. Klimov, A. A. Mikhailovsky, D. W. McBranch, C. A. Leatherdale, and M. G. Bawendi, "Mechanisms for intraband energy relaxation in semiconductor quantum dots: The role of electron-hole interactions," Phys. Rev. B **61**, R13349 (2000).
[122]W. Yang, H. Lee, T. J. Johnson, P. C. Sercel, and A. G. Norman, "Electronic structure of self-organized InAs/GaAs quantum dots bounded by {136} facets," Phys. Rev. B **61**, 2784 (2000).
[123]V. S. Williams, G. R. Olbright, B. D. Fluegel, S. W. Koch, and N. Peyghambarian, "Optical nonlinearities and ultrafast carrier dynamics in semiconductor doped glasses," J. Mod. Opt. **35**, 1979–1993 (1988).
[124]A. Kojima, K. Teshima, Y. Shirai, and T. Miyasaka, "Organometal halide perovskites as visible-light sensitizers for photovoltaic cells," J. Am. Chem. Soc. **131**, 6050–6051 (2009).
[125]J.-H. Im, C.-R. Lee, J.-W. Lee, S.-W. Park, and N.-G. Park, "6.5% efficient perovskite quantum-dot-sensitized solar cell," Nanoscale **3**, 4088–4093 (2011).
[126]H.-S. Kim, C.-R. Lee, J.-H. Im, K.-B. Lee, T. Moehl, A. Marchioro, S.-J. Moon, R. Humphry-Baker, J.-H. Yum, J. E. Moser, M. Grätzel, and N.-G. Park, "Lead iodide perovskite sensitized all-solid-state submicron thin film mesoscopic solar cell with efficiency exceeding 9%," Sci. Rep. **2**, 591 (2012).
[127]M. M. Lee, J. Teuscher, T. Miyasaka, T. N. Murakami, and H. J. Snaith, "Efficient hybrid solar cells based on meso-superstructured organometal halide perovskites," Science **338**, 643–647 (2012).
[128]J. Burschka, N. Pellet, S.-J. Moon, R. Humphry-Baker, P. Gao, M. K. Nazeeruddin, and M. Grätzel, "Sequential deposition as a route to high-performance perovskite-sensitized solar cells," Nature **499**, 316–319 (2013).
[129]M. M. Liu, M. B. Johnston, and H. J. Snaith, "Efficient planar heterojunction perovskite solar cells by vapour deposition," Nature **501**, 395–398 (2013).
[130]H. J. Snaith, "Perovskites: the emergence of a new era for low-cost, high-efficiency solar cells," J. Phys. Chem. Lett. **4**(21), 3623–3630 (2013).
[131]L. Xu, X. Chen, J. Jin, W. Liu, B. Dong, X. Bai, H. Song, and P. Reiss, "Inverted perovskite solar cells employing doped NiO hole transport layers: A review," Nano Energy **63**, 103860 (2019).
[132]H. J. Snaith, "Present status and future prospects of perovskite photovoltaics," Nat. Mater. **17**(5), 372–376 (2018).
[133]G. E. Eperon, M. T. Hörantner, and H. J. Snaith, "Metal halide perovskite tandem and multiple-junction photovoltaics," Nat. Rev. Chem. **1**(12), 0095 (2017).
[134]D.-H. Kang and N.-G. Park, "On the current-voltage hysteresis in perovskite solar cells: Dependence on perovskite composition and methods to remove hysteresis," Adv. Mater. **31**, 1805214 (2019).
[135]N.-G. Park, *Advanced Concepts in Photovoltaics* (RSC, Cambridge, 2014), Vol. 242, Chap. 7.
[136]A. K. Jena, A. Kulkarni, and T. Miyasaka, "Halide perovskite photovoltaics: Background, status, and future prospects," Adv. Funct. Mater. **119**(5), 3036–3103 (2018).
[137]Y. T. Huang, S. Kavanagh, D, Scanlon, A. Walsh, and R. Hoye, "Perovskite-inspired materials for photovoltaics and beyond from design to devices," Nanotech. **32**(13), 132004 (2021).
[138]F. Giustino and H. J. Snaith, "Toward lead-free perovskite solar cells," ACS Energy Lett. **1**(6), 1233–1240 (2016).
[139]W. A. Dunlap-Shohl, Y. Zhou, N. P. Padture, and D. B. Mitzi, "Synthetic approaches for halide perovskite thin films," Chem. Rev. **119**(5), 3193–3295 (2019).
[140]H.-S. Kim, A. Hagfeldt, and N.-G. Park, "Morphological and compositional progress in halide perovskite solar cells," Chem. Comm. **55**(9), 1192–1200 (2019).
[141]Y. Yang, D. P. Ostrowski, R. M. France, K. Zhu, J. van de Lagemaat, J. M. Luther, and M. C. Beard, "Observation of a hot-phonon bottleneck in lead-iodide perovskites," Nat. Photon. **10**(1), 53–59 (2016).
[142]S. Kahmann and M. A. Loi, "Hot carrier solar cells and the potential of perovskites for breaking the Shockley-Queisser limit," J. Mater. Chem. C **7**, 2471–2486 (2019).
[143]M. Li, J. Fu, Q. Xu, and T. C. Sum, "Slow hot-carrier cooling in halide perovskites: Prospects for hot carrier solar cells," Adv. Mater. **31**, 1802486 (2019).

[144]M. Li, S. Bhaumik, T. Goh *et al.*, "Slow cooling and highly efficient extraction of hot carriers in colloidal perovskite nanocrystals," Nat Comm. **8**, 14350 (2017).
[145]P. P. Joshi, S. F. Maehriein, and X. Y. Zhu, "Dynamic screening and slow cooling of hot carriers in lead halide perovskites," Adv. Mater **31**(47), 1803054 (2019).
[146]J. Fu, Q. Xu, G. Han, B. Wu, C. H. A. Huan, M. L. Leek, and T. C. Sum, "Hot carrier cooling mechanism in halide perovskites", Nat. Commun. **8**, 1300 (2017).
[147]A. J. Nozik, R. J. Ellingson, O. I. Micic, J. L. Blackburn, P. Yu, J. E. Murphy, M. C. Beard, and G. Rumbles, "Unique approaches to solar photon conversion based on semiconductor nanostructures and novel molecular chromophores; dynamics of electron relaxation, interfacial charge transfer, and carrier multiplication," in *Proceedings of the. 27th DOE Solar Photochem. Research Conf.* (Airlie Conf. Ctr., Warrenton, VA, 2004), available at https://science.osti.gov/bes/csgb/Principal-Investigators-Meetings.
[148]J. Burdett, A. M. Müller, D. Gosztola, and C. J. Bardeen "Excited state dynamics in solid and monomeric tetracene: The roles of superradiance and exciton fission," J. Chem. Phys. **133**, 144506 (2010).
[149]J. Lee, P. Jadhav, and M. A. Baldo, "High efficiency organic multilayer photodetectors based on singlet exciton fission," App. Phys. Lett. **95**, 033301 (2009).
[150]J. C. Johnson, A. J. Nozik, and J. Michl, "The role of chromophore coupling in singlet fission," Acc. Chem. Res. **46**, 1290–1299 (2013).
[151]A. Rao, M. W. B. Wilson, J. M. Hodgkiss, S. Albert-Seifried, H. Bässler, and R. H. Friend, "Exciton fission and charge generation via triplet excitons in pentacene/C60 bilayers," J. Am. Chem. Soc. **132**, 12698–12703 (2010).
[152]S. Ito, T. Nagami, and M. Nakano, "Molecular design for efficient singlet fission," J. Photochem. Photobiol. C: Photochem. Rev. **34**, 85–120 (2018).
[153]K. Miyata, F. S. Conrad-Burton, F. L. Geyer, and X.-Y. Zhu, "Triplet pair states in singlet fission," Chem. Rev. **119**, 4261–4292 (2019).
[154]D.-T. Nguyen, L. Lombez, F. Gibelli, S. Boyer-Richard, A. Le Corre, O. Durand, and J. F. Guillemoles, "Quantitative experimental assessment of hot carrier-enhanced solar cells at room temperature," Nat. Energy **3**, 236–242 (2018).
[155]A. J. Nozik, in "*Photoelectrochemical Water Splitting*", edited by H-J Lewerenz and L. Peter (Royal Society of Chemistry, Cambridge, 2013), Chap. 13. pp. 379–385.
[156]R. Memming, "*Semiconductor Electrochemistry*" (Wiley-VCH, Weinham, 2000).
[157]H. Gerischer, in "*Photovoltaic and Photoelectrochemical Solar Energy Conversion*", edited by F. Cardon, W. P. Gomes, and W. Dekeyser (NATO Advanced Study Institute, Plenum, New York, 1981).
[158]H.-J. Lewerenz and L. Peter, in *Photoelectrochemical Water Splitting* (Royal Society of Chemistry, Cambridge, 2013).
[159]A. J. Nozik and R. Memming, "Physical chemistry of semiconductor-liquid interfaces," J. Phys. Chem. **100**, 13061–13078 (1996).
[160]N. S. Lewis, "Mechanistic studies of light-induced charge separation at semiconductor/liquid interfaces," Acc. Chem. Res. **23**, 175–183 (1990).